magnetochemistry

MDPI

Article

Nonequivalent Antiferromagnetically Coupled Sublattices Induce Two-Step Spin-Crossover Transitions: Equilibrium and Nonequilibrium Aspects

Valon Veliu [1,*], Orhan Yalçın [2], Songül Özüm [3] and Rıza Erdem [4]

[1] Faculty of Electrical and Computer Engineering, University of Prishtina, 10000 Prishtinë, Kosovo
[2] Department of Physics, Niğde Ömer Halisdemir University, 51240 Niğde, Türkiye; yalcin@ohu.edu.tr
[3] Alaca Avni Çelik Vocational School, Hitit University, 19600 Çorum, Türkiye; songulozum@hitit.edu.tr
[4] Department of Physics, Akdeniz University, 07058 Antalya, Türkiye; rerdem@akdeniz.edu.tr
* Correspondence: valon.veliu@uni-pr.edu

Abstract: As a continuation to the previously published work (Yalçın et al. (2022)), we investigate the equilibrium and nonequilibrium properties of the spin-crossover systems, with a specific focus on the nonequivalent sublattice, and compare these properties with those of the equivalent sublattices. We used the lowest approximation of the cluster variation method (LACVM) to derive the static equations for the order parameters of the two sublattices and determine high-spin fraction in relation to temperature and external magnetic field in a spin-crossover system. At a low temperature, the transition from stable high-spin (HS) state where $n_{HS} = 1$ occurs in the plateau region, where $n_{HS} = 0.5$ for nonequivalent sublattices. The order parameters for non-equivalent sublattices exhibit different states at the transition temperature. Also, we study the nonequilibrium properties of the order parameters and high-spin fraction using the path probability method (PPM). With the current model, we obtain and analyze the relaxation curves for the order parameters S_a, S_b, and high-spin fraction. These curves demonstrate the existence of bistability at low temperatures. At the end of this study, we present the flow diagram that shows the order parameters for different temperature values. The diagram exhibits states that are stable, metastable, and unstable.

Keywords: nonequivalent sublattice; spin-crossover system; two-sublattice; equilibrium and nonequilibrium properties

check for updates

Citation: Veliu, V.; Yalçın, O.; Özüm, S.; Erdem, R. Nonequivalent Antiferromagnetically Coupled Sublattices Induce Two-Step Spin-Crossover Transitions: Equilibrium and Nonequilibrium Aspects. *Magnetochemistry* **2024**, *10*, 42. https://doi.org/10.3390/magnetochemistry10060042

Academic Editor: Zheng Gai

Received: 27 April 2024
Revised: 27 May 2024
Accepted: 30 May 2024
Published: 4 June 2024

Copyright: © 2024 by the authors. Licensee MDPI, Basel, Switzerland. This article is an open access article distributed under the terms and conditions of the Creative Commons Attribution (CC BY) license (https://creativecommons.org/licenses/by/4.0/).

1. Introduction

Spin-crossover (SCO) systems have attracted significant attention because of their potential application to memory devices, molecular sensors, and displays, as well as to recent developments related to the barocaloric effect and refrigerant effect [1–5]. The SCO phenomenon refers to the transition between two molecular spin states: the low-spin state (LS), which is diamagnetic, and the high-spin state (HS), which is paramagnetic. The LS state is energetically favorable and dominates at low temperatures, whereas the HS state dominates at high temperatures due to its favorable energy. This transition specifically occurs in first-row transition metal complexes with an electronic configuration ranging from d^4 to d^7. Research has shown that the spin transitions in spin-crossover materials can be controlled by applying external stimuli, including changes in temperature, pressure, light irradiation (electromagnetic irradiation), magnetic or electric field, etc., [6–14]. Their thermodynamic bistability remains a subject of great interest due to their potential applications [15–17]. Furthermore, SCO materials display a diverse range of thermodynamic phenomena that lead to alterations in magnetic, optical, and mechanical characteristics. These changes serve as the basis for extensive and comprehensive experimental investigations [18–20].

In many investigations, it has been observed that, when spin-crossover systems are exposed to light in the green to red wavelength range, they complete a spin transition from

a low spin state to a high spin state, even at low temperatures. The process that has been described is referred to as light-induced excited spin state trapping [21–27]. Furthermore, both experimental and theoretical studies have documented the presence of light-induced hidden hysteresis and bistability in spin transitions, as reported in the references [28]. In addition, the application of pressure plays an important role as an external stimulus [29,30]. Some SCO systems change from first-order transitions to continued transitions or incomplete transitions [31].

Various types of models have been used to represent SCO systems from a theoretical perspective. The Ising-like Hamiltonian model is commonly used to study the SCO phenomenon. The properties of the SCO system have been investigated by examining this model using various techniques, including the mean field approach, Bethe Peierls approximation, general stochastic dynamics developed by Glauber, Monte Carlo methods, Arrhenius transition probability, transfer matrix, local equilibrium, etc. A number of these methods have effectively reproduced the experimentally observed spin-crossover transitions [32–48].

In this work, we extend our previously published work [49] with a focus on nonequivalent sublattices. We study the equilibrium and nonequilibrium properties of the system using the lowest approximation of the cluster variation method (LACVM) [50] and the path probability method (PPM) [51]. The Ising-like Hamiltonian model that we have analyzed for SCO systems considers both equivalent and nonequivalent sublattices. We first investigate the thermodynamic properties for different values of the intersublattice and intrasublattice interaction parameters, ligand field energy, and degeneracy. Additionally, we present the magnetic evolution of the order parameters and the high-spin fraction at various fixed temperatures. For nonequivalent sublattices in the warming process, we found that the high-spin fraction n_{HS} displayed a stable HS state in the low temperature region and jumped to the intermediate metastable/stable state HS-LS at $n_{HS} = 0.5$. The relaxation curves of the order parameters and high-spin fraction with bistable states were observed. For the same initial values of the order parameters, two-step relaxation curves are present. The flow diagram of the order parameters at T = 60 for nonequivalent sublattices shows two stable states, two unstable states, and metastable states. Our results are in agreement with other experimental and theoretical findings. The self-consistent equation of the system was performed using the Newton–Raphson and Runge–Kutta methods.

The present work is organized as follows: Section 2 describes the model briefly and presents the derivations of static and dynamic equations. In Section 3, we obtain the numerical results and offer a discussion. In Section 4, we end with a conclusion.

2. Description of the Model and Derivations of Static and Dynamic Equations

In order to describe the two-step spin-crossover systems, an Ising-like Hamiltonian with ferromagnetic intrasublattice interactions ($J_a > 0$, $J_b > 0$) and antiferromagnetic intersublattice interactions ($J_{ab} < 0$) was introduced in [32,52] as follows:

$$\mathcal{H} = -J_a \sum_{\langle i,j \rangle} S_i^a S_j^a - J_b \sum_{\langle i,j \rangle} S_i^b S_j^b - J_{ab} \sum_{\langle i,j \rangle} S_i^a S_j^b + h \sum_{\langle i,j \rangle} \left(S_i^a + S_i^b \right) + H \sum_{\langle i,j \rangle} \left(S_i^a + S_i^b \right). \quad (1)$$

where $S_i^a = S_j^a = \pm 1$, $S_i^b = S_j^b = \pm 1$, $h = \frac{\Delta}{2} - \frac{k_B T}{2} \ln g$ (Δ is the ligand field energy, $g = g_{HS}/g_{LS}$ is the degeneracy, T is the absolute temperature, and k_B $(= 1)$ the Boltzmann constant). All exchange coupling parameters appearing in Equation (1) are in units of $k_B T$. In the presence of an external magnetic field H, the Zeeman effect is considered ($H = g\mu B$, μ is the Bohr magneton and B the applied magnetic field [39]). Generally, g depends on temperature through the temperature dependence of the phonon density of the lattice [39,40]. Sublattice order parameters are defined as:

$$S_a = \langle S_i^a \rangle = X_1^a - X_2^a \text{ and } S_b = \left\langle S_j^b \right\rangle = X_1^b - X_2^b \quad (2)$$

where X_1^a and X_1^b are average fractional values of each spin state with value $+1$ on a and b sublattices, respectively, while X_2^a and X_2^b are average fractional value of each spin state with value -1 on a and b sublattices, respectively. By solving Equation (1), Helmholtz free energy can be expressed in terms of sublattice order parameters defined as follows:

$$\begin{aligned}\Phi = \frac{\beta F}{N} = \frac{\beta}{N}[-J_a(S_a)(S_a) - J_b(S_b)(S_b) - J_{ab}(S_a)(S_b) + h(S_a + S_b) + H(S_a + S_b)] \\ +\tfrac{1}{2}(1+S_a)\ln\tfrac{1}{2}(1+S_a) \\ +\tfrac{1}{2}(1-S_a)\ln\tfrac{1}{2}(1-S_a) + \tfrac{1}{2}(1+S_b)\ln\tfrac{1}{2}(1+S_b) + \tfrac{1}{2}(1-S_b)\ln\tfrac{1}{2}(1-S_b)\end{aligned} \tag{3}$$

where $\beta = 1/k_B T$, F $\left(F = E - TS_{entropy}\right)$ is the free energy and N $(N = N_a + N_b)$ presents the total number of points on sublattices. After using the LACVM [50], one can obtain the following self-consistent equations for two sublattices to investigate the static properties:

$$\begin{aligned}S_a &= \frac{e^{\beta(-2J_aS_a - J_{ab}S_b + h + H)} - e^{\beta(2J_aS_a + J_{ab}S_b - h - H)}}{e^{\beta(-2J_aS_a - J_{ab}S_b + h + H)} + e^{\beta(2J_aS_a + J_{ab}S_b - h - H)}}, \\ S_b &= \frac{e^{\beta(-2J_bS_b - J_{ab}S_a + h + H)} - e^{\beta(2J_bS_b + J_{ab}S_a - h - H)}}{e^{\beta(-2J_bS_b - J_{ab}S_a + h + H)} + e^{\beta(2J_bS_b + J_{ab}S_a - h - H)}}.\end{aligned} \tag{4}$$

After some calculations from Equation (4), and after applying the two possible values of the spin states [53], we can find the following:

$$\begin{aligned}S_a &= \frac{-1 + \exp[-\beta\Delta E_a]}{1 + \exp[-\beta\Delta E_a]}, \\ S_b &= \frac{-1 + \exp[-\beta\Delta E_b]}{1 + \exp[-\beta\Delta E_b]},\end{aligned} \tag{5}$$

with

$$\begin{aligned}\Delta E_a &= -4J_aS_a - 2J_{ab}S_b + 2h + 2H, \\ \Delta E_b &= -4J_bS_b - 2J_{ab}S_a + 2h + 2H.\end{aligned} \tag{6}$$

The order parameters S_a and S_b for each sublattice are directly related to the high-spin fraction n_{HS} of a spin-crossover system defined as:

$$n_{HS} = \frac{1+S}{2} \tag{7}$$

where $S = \frac{S_a + S_b}{2}$.

In order to study the dynamic aspects of the above spin system, one can obtain dynamic equations by using the path probability method introduced by Kikuchi [51]. In the PPM, the rate of change of a state variable is written as:

$$\frac{dX_i}{dt} = \sum_{i \neq j}\left(X_{ji} - X_{ij}\right) \tag{8}$$

where X_{ij} is the path probability rate for the system to go from state i to state j, with $X_{ij} = X_{ji}$.

For the rates X_{ij}, we use the following recipe, called recipe II, introduced by Kikuchi:

$$X_{ij} = k_{ij} Z^{-1} X_i \exp\left(-\beta \frac{\partial E}{\partial X_j}\right) \tag{9}$$

where k_{ij} is the rate constants, with $k_{ij} = k_{ji}$, Z is the partition function, and E is the internal energy of the system. The partition function Z is calculated for the Hamiltonian model (1), and, for the two sublattices, it can be written as:

$$\begin{aligned} Z_a &= \sum_{i=1}^{2} e_i^a \\ Z_b &= \sum_{j=1}^{2} e_j^b \end{aligned} \tag{10}$$

where, after many calculations, we found that $e_1^a = e^{\beta(-2J_aS_a - J_{ab}S_b + h + H)}$ and $e_2^a = e^{\beta(2J_aS_a + J_{ab}S_b - h - H)}$ for sublattice a and $e_1^b = e^{\beta(-2J_bS_b - J_{ab}S_a + h + H)}$ and $e_2^b = e^{\beta(2J_bS_b + J_{ab}S_a - h - H)}$ for sublattice b. The dynamic equations for two sublattices can be written as:

$$\begin{aligned} \frac{Z_a}{k_1}\frac{dS_a}{dt} &= 2\left(X_2^a e_1^a - X_1^a e_2^a\right) \\ \frac{Z_b}{k_1}\frac{dS_b}{dt} &= 2\left(X_2^b e_1^b - X_1^b e_2^b\right) \end{aligned} \tag{11}$$

or

$$\begin{aligned} \frac{Z_a}{k_1}\frac{dS_a}{dt} &= 2\sinh\beta(-2J_aS_a - J_{ab}S_b + h + H) - 2S_a\cosh\beta(-2J_aS_a - J_{ab}S_b + h - H), \\ \frac{Z_b}{k_1}\frac{dS_b}{dt} &= 2\sinh\beta(-2J_bS_b - J_{ab}S_a + h + H) - 2S_b\cosh\beta(-2J_bS_b - J_{ab}S_a + h + H). \end{aligned} \tag{12}$$

From Equation (12), after many calculations, and after applying the two possible values of the spin states as in the static part, we can obtain the dynamic equation for the order parameters:

$$\begin{aligned} \frac{1}{k_1}\frac{dS_a}{dt} &= \frac{-1+e^{\beta(-4J_aS_a - 2J_{ab}S_b + 2h + 2H)}}{+1+e^{\beta(-4J_aS_a - 2J_{ab}S_b + 2h + 2H)}} - S_a \\ \frac{1}{k_1}\frac{dS_b}{dt} &= \frac{-1+e^{\beta(-4J_bS_b - 2J_{ab}S_a + 2h + 2H)}}{+1+e^{\beta(-4J_bS_b - 2J_{ab}S_a + 2h + 2H)}} - S_b \end{aligned} \tag{13}$$

where k_1 is the rate constant. If we take $\frac{dS_a}{dt} = 0$ and $\frac{dS_b}{dt} = 0$, the above equations return Equation (4) that present static equations.

3. Results and Discussion

In this section, we computed results using the static and dynamic equations that were introduced in the previous section. First, we are going to investigate how the intersublattice parameter, intrasublattice parameter, degeneracy, ligand field energy, and external magnetic field influence the phase transition properties of a spin-crossover system. In the analysis of equilibrium properties, we examine both the equivalent and nonequivalent sublattices. Second, we compute results for the nonequilibrium properties of the system.

3.1. Static Behaviors

Figure 1 shows the temperature evolution of the order parameters (S_a, S_b) and high-spin fraction (n_{HS}) for different selected values of the intersublattice interaction parameter (J_{ab}) in the case of equivalent ($J_a = J_b$) and nonequivalent ($J_a \neq J_b$) sublattices. For equivalent sublattices in Figure 1a, the order parameter transition was gradual when the intersublattice interaction parameter (J_{ab}) was weak. As the value of J_{ab} increased, the interaction between the two sublattices became stronger, leading to a first-order transition characterized by a hysteresis of the order parameters. This property was observed when the reduced temperature was increased and when it was decreased. While increasing the coupling parameter (J_{ab}) values, the width of the hysteresis became enlarged. The thermal behavior of the high-spin fraction n_{HS} depends on the J_{ab}, plotted in Figure 1b. For small values of the coupling parameter $J_{ab} = -400$ (orange curve) and -300 (green curve), the SCO transition was gradual. The thermal properties of the high-spin fraction n_{HS} underwent a change in shape as J_{ab} increased, i.e., $J_{ab} = -200$ (magenta curve), -100 (red curve), or -50 (blue curve), and the transition of the spin-crossover (SCO) exhibited thermal hysteresis. By increasing the coupling parameter J_{ab}, the width of the hysteresis became expanded, as demonstrated by the simulations performed for the order parameters (S_a, S_b).

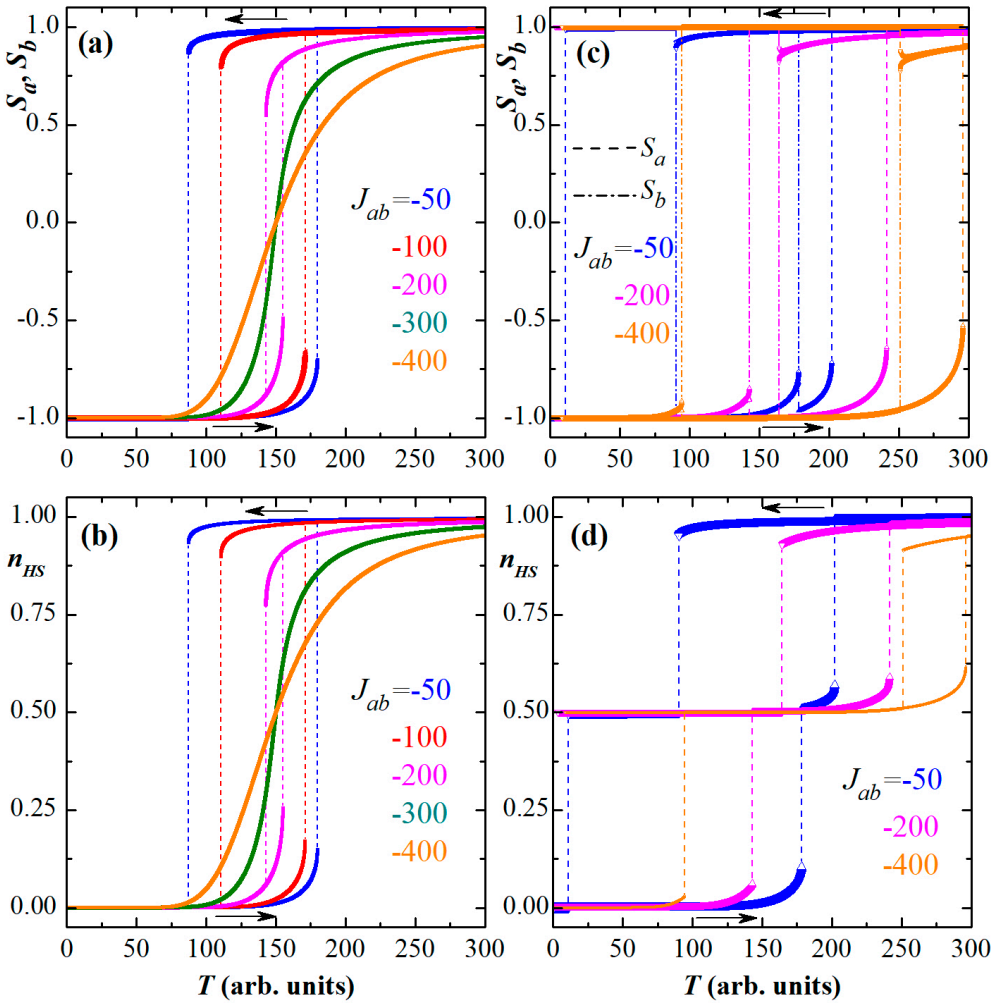


Figure 1. Thermal behaviors of the order parameters S_a, S_b, and high-spin fraction n_{HS} in the absence of the external magnetic field for different selected values of the intersublattice parameter (J_{ab}). In panels (**a**,**b**), $J_a = J_b = 200$, that is, the sublattices are equivalent, while, in panels (**c**,**d**), $J_a = 200$ and $J_b = 199$, that is, the sublattices are nonequivalent. Other parameters are the same: $\Delta = 900$, g = 400, and $H = 0.0$.

Figure 1c,d display the phase transitions of the order parameters and the high-spin fraction n_{HS} for nonequivalent sublattices. The sublattices had different values of $J_a = 200$ and $J_b = 199$. These phase transitions are shown for specific values of the intersublattice interaction parameter (J_{ab}). We analyzed the phase transition of order parameters and the high-spin fraction for $J_{ab} = -50$ (indicated by the blue curve) in order to explain the intermediate plateau region for the high-spin fraction n_{HS}. At low temperatures, the order parameters of two sublattices, S_a and S_b, were both equal to -1, indicating a low-spin state. As the temperature increased, the order parameters remained the same until a bifurcation occurred at $T^{\uparrow} \sim 177.9$. At this point, the order parameter of sublattice b underwent a first-order phase transition from $S_b = -0.78$ (low-spin LS state) to $S_b = 1$ (high-spin HS state). The order parameter of sublattice a remained in a low-spin state until the temperature reached approximately $T^{\uparrow} \sim 202.7$, at which point it underwent a first-order phase transition from $S_a = -0.72$ (LS state) to $S_a = 1$ (HS state). At temperatures above $T^{\uparrow} \sim 202.7$, both sublattices became equivalent again. During the cooling process, a comparable situation arose where the breaking of the symmetry between the two sublattices occurred at a temperature of $T^{\downarrow} \sim 90.2$. This was when the order parameter of sublattice b underwent a first-order phase transition from $S_b = 0.9$ (HS state) to $S_b = -1$ (LS state). The order parameter of sublattice a remained in a high-spin state until the temperature

reached around $T^{\downarrow} \sim 10.6$. At this temperature, it underwent a first-order phase transition from $S_a = 1$ (HS state) to $S_a = -1$ (LS state). At temperatures below $T^{\downarrow} \sim 10.6$, both sublattices exhibited the same state, which is referred to as an LS state. When the J_{ab} values decreased, we observed that the order parameters S_a and S_b exhibited similar properties for the warming process. It is important to emphasize that the value of S_a (=1) remained constant during the cooling process, and no phase transition was observed for J_{ab} values of -200 (magenta curve) and -400 (orange curve) from $S_a = 1$ to $S_a = -1$ as it appeared for S_b.

The high-spin fraction n_{HS} for the nonequivalent sublattices (Figure 1d) exhibited an abrupt (first-order phase transition) behavior, with two steps and separate branches in the plateau region between the hysteresis loop during both the warming and cooling processes. This phenomenon is also supported by the experimental and theoretical study of $\left[\mathrm{Fe^{II}}(5-\mathrm{NO_2}-\mathrm{sal}-\mathrm{N}(1,4,7,10))\right]$ [54]. The properties of n_{HS} for $J_{ab} = -50$ (blue curve) arose due to the presence of various combinations of spin states on the plateau ($n_{HS} = \frac{1}{2}$). The order parameters (S_a, S_b) exhibited different spin states during the heating process, from $T_{1/2}$ ~177.9 to ~202.7, as discussed in Figure 1c. During the cooling process, the high-spin fraction n_{HS} exhibited similar properties. There were different combinations of spin states on the plateau ($n_{HS} = \frac{1}{2}$), with values ranging from $T_{1/2} \sim 90.2$ to ~10.6 . While J_{ab} values decreased, the transition became two-stepped with the presence of hysteresis. The width of the hysteresis loop in the second step was slightly reduced with decreasing J_{ab} (-200 and -400), and the whole cycle was shifted to relatively high temperatures. At very low temperatures in cooling mode, an incomplete spin transition was present on the plateau ($n_{HS} = \frac{1}{2}$) for both J_{ab} values. The selected value parameters are presented in the figure caption.

Next, we studied the thermal properties of the order parameters S_a, S_b, and high-spin fraction n_{HS} without an external magnetic field for various chosen values of intrasublattice parameters (J_a, J_b). In Figure 2a,b, $J_a = J_b$ are equivalent sublattices, whereas, in Figure 2c,d, $J_a \neq J_b$ are non-equivalent sublattices. When the coupling parameters were small, such as $J_a = J_b = 15$ and 50 for equivalent sublattices and $J_a = 15$ and $J_b = 14$ for nonequivalent sublattices, the transition was gradual and hysteresis was not observed. When the intrasublattice parameter increased to values such as $J_a = J_b = 80$ and 100, a first-order transition occurred, leading to hysteresis during the warming and cooling processes. This was observed for the order parameters S_a, S_b, and for the high-spin fraction n_{HS}.

When the sublattices were nonequivalent, with $J_a = 50$ and $J_b = 49$ (magenta curve), the order parameter transitions were first-order, resulting in hysteresis between the warming and cooling processes. The high-spin fraction n_{HS} transition occurred in two steps and exhibited hysteresis between the warming and cooling processes. Increasing the J_a and J_b values resulted in a first-order transition that shifted to lower temperatures, as depicted in Figure 2. The intrasublattice coupling parameter has been addressed in different theoretical models [52,55]. The additional parameters utilized in our theoretical model are: $J_{ab} = -15$, $\Delta = 400$, g = 100 and $H = 0.0$.

Figure 3 shows the temperature dependence of the S_a, S_b, and n_{HS} for four different values of degeneracy in the absence of an external magnetic field. As it is shown in Figure 3a,b, in the case of equivalent sublattices ($J_a = J_b = 50$), the transition was first-order for large values of g (1000/magenta curve and 5000/green curve) and the whole hysteresis shifted to a lower temperature region. When the degeneracy became g (100/red curve and 10/blue curve), the hysteresis disappeared and the transition became gradual and shifted to the higher temperature side. We can conclude that, for small values of g, the transition is gradual and shifted to the high temperature side.

In the case of nonequivalent sublattices, when the intrasublattice parameters were $J_a = 51$ and $J_b = 50$, the transition was first-order for S_a, S_b, while, for n_{HS}, it was first-order with two steps, as depicted in Figure 3c,d. The high-spin fraction n_{HS} shifted to the left (lower temperature) as the degeneracy g increased. For non-equivalent sublattices, we found three typical two-step transitions during the warming and cooling processes for

the high-spin fraction for the selected values: (I) first-order transition with the presence of hysteresis at the lower transition temperature and gradual transition at the higher transition temperature when g = 10; (II) first-order transition with the presence of hysteresis at the lower and higher transition temperature when g = 100; (III) first-order transition with a hidden, stable low-spin state that remained stable until T = 30 during the warming, and an incomplete spin transition on the plateau during the cooling processes at the lower transition temperature. The first-order transition with the presence of hysteresis during the warming and cooling processes at the higher transition temperature was present in the case of g = 1000. Similar properties were found for n_{HS} in the case of g = 5000. Parameter values are given in the text of the figure caption.

Figure 4 displays the temperature dependence of the order parameters S_a, S_b, and high-spin fraction n_{HS} for different values of ligand field energy in the absence of an external magnetic field. It is interesting to emphasize that, for equivalent sublattices in Figure 4a,b, the order parameters S_a, S_b, and the high-spin fraction n_{HS} displayed a stable high-spin (HS) state in the low temperature region and jumped to relax the low-spin state, where $\Delta = 85$/blue curve, when the temperature increased. During the transition from a low-spin (LS) state to a high-spin (HS) state, a thermal hysteresis loop appeared in the warming and cooling phases.

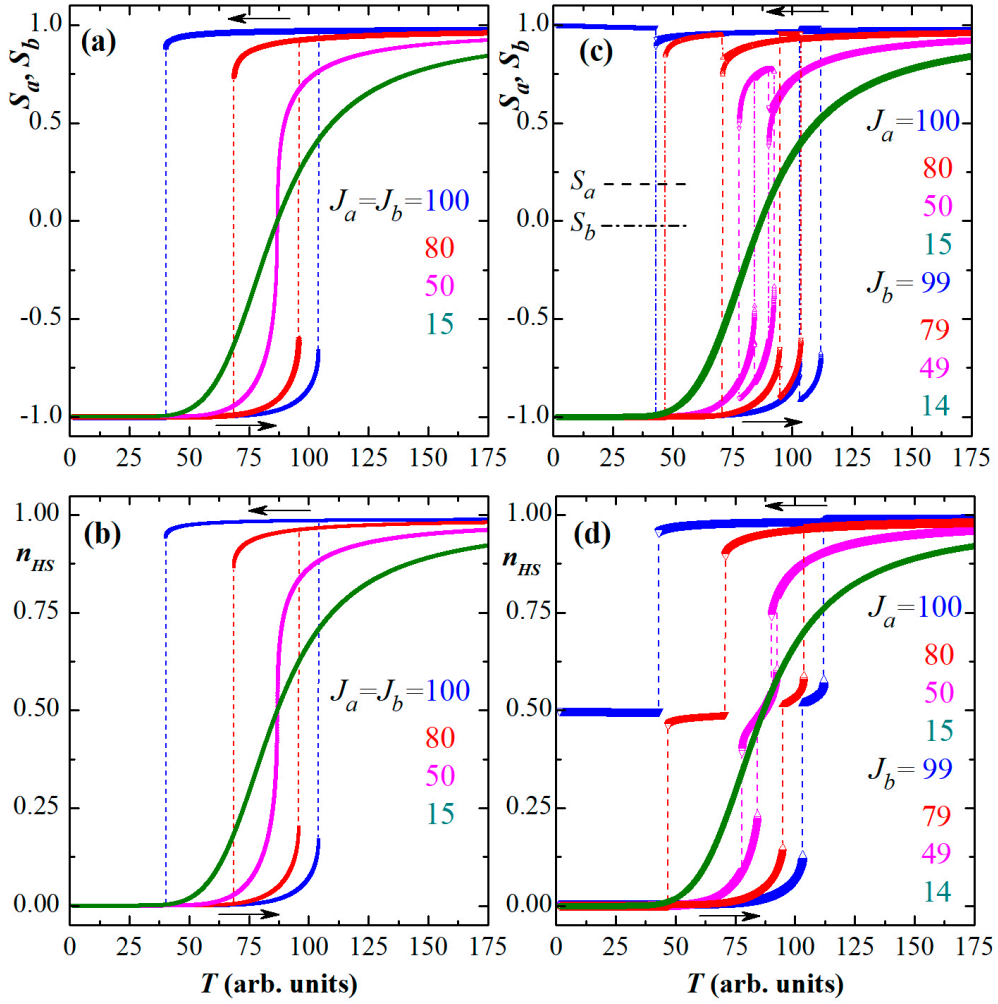


Figure 2. Thermal behaviors of the order parameters S_a, S_b, and high-spin fraction n_{HS} in the absence of the external magnetic field for different selected values of the intrasublattice parameter (J_a, J_b). In panels (**a**,**b**), $J_a = J_b$, that is, the sublattices are equivalent, while, in panels (**c**,**d**), $J_a \neq J_b$, that is, the sublattices are nonequivalent. Other parameters are the same: $J_{ab} = -15$, $\Delta = 400$, g = 100, and $H = 0.0$.

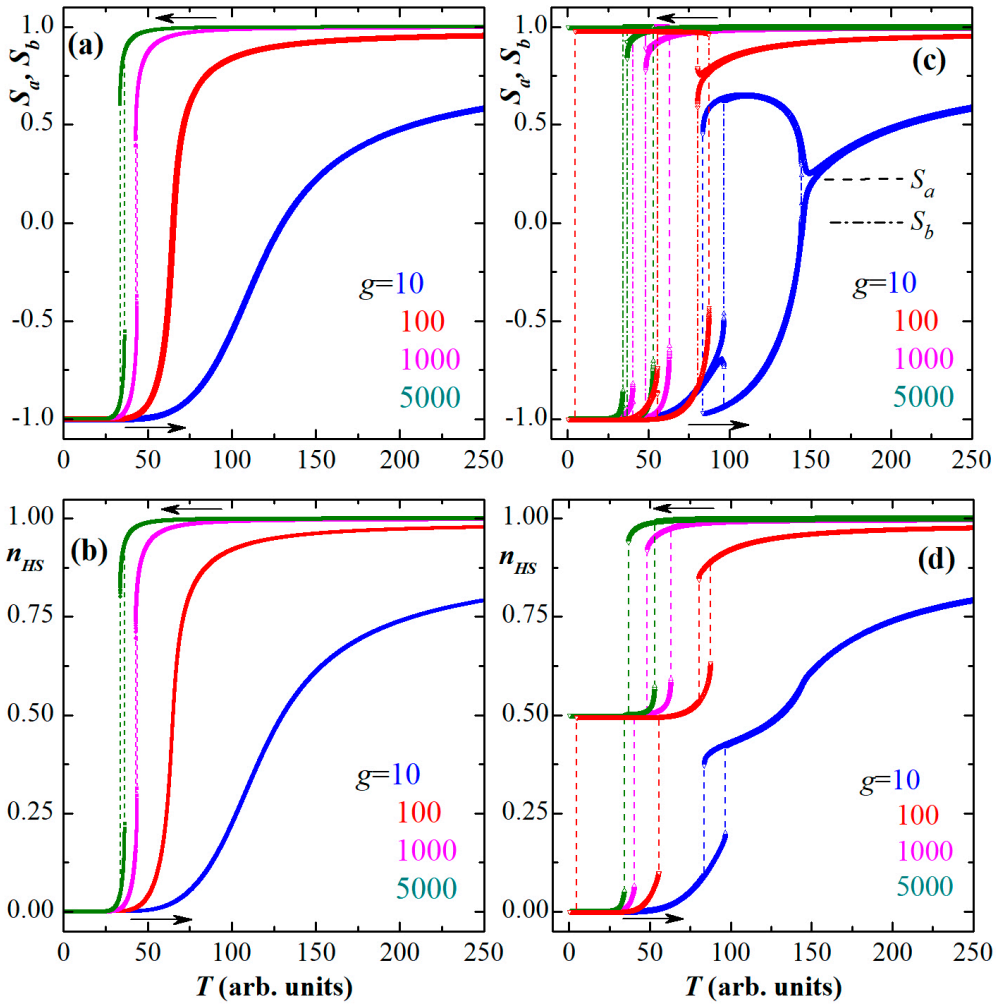


Figure 3. Thermal behaviors of the order parameters S_a, S_b, and high-spin fraction n_{HS} in the absence of the external magnetic field for different selected values of the degeneracy parameter (g). In panels (**a**,**b**), $J_a = J_b = 50$, that is, the sublattices are equivalent, while, in panels (**c**,**d**), $J_a = 51$ and $J_b = 50$, that is, the sublattices are nonequivalent. Other parameters are the same: $J_{ab} = -50$, $\Delta = 300$, and $H = 0.0$.

The existence of this phenomenon was theoretically predicted by Miyashita et al. [56] and confirmed also by an experimental study on $Rb_{0.64}Mn[Fe(CN)_6]_{0.88}{\cdot}1.7H_2O$ [57]. Other theoretical studies have also observed this phenomenon when investigating the spin-crossover transition of Co–Fe Prussian blue analogs [58]. A study of pressure-induced phase transitions in SCO materials also confirmed the presence of a metastable state at low temperatures [30]. The stable high-spin state was not observed in the low temperature region for $\Delta = 105$/red curve, the transition was abrupt, and the hysteresis was present. When the ligand field energy became larger, e.g., $\Delta = 125$/green curve, the transition was gradual, and the stable state and hysteresis loop were not observed.

The nonequivalent sublattices for $J_a = 51$ and $J_b = 50$ and different values of ligand field energy are shown in Figure 4c,d. The transition of the order parameter S_a, for $\Delta = 85$/blue curve, in the heating and cooling processes was located between 0.8 and 1.0, with the presence of hysteresis. The hysteresis value was $\Delta T = T^{\uparrow} - T^{\downarrow} = 26$. Sublattice b exhibited a first-order transition of the order parameter S_b with the presence of hysteresis and also exhibited the same value ($\Delta T = 26$) as that of S_a. The transition for S_b occurred between -1.0 and 0.79. For $\Delta = 105$/red curve, the transition became abrupt, and the hysteresis loops narrowed and shifted to a larger temperature region. When Δ became larger ($= 125$/green curve), at low temperatures, the order parameters of the two

sublattices, S_a and S_b, became equal to -1, indicating a low-spin state. As the temperature increased, the order parameters remained the same until $T^{\uparrow} \sim 43$. At this point, the order parameter of sublattice b underwent a first-order phase transition from $S_b = -0.8$ (LS state) to $S_b = 1$ (HS state). The order parameter of sublattice a remained in a low-spin state until the temperature reached approximately $T^{\uparrow} \sim 95.4$, at which point it underwent a first-order phase transition from $S_a = -0.36$ (LS state) to $S_a = 0.68$ (HS state). At higher temperatures, both sublattices became equivalent. The value of S_a during the cooling process remained in a high-spin state at low temperatures, and no phase transition was observed from $S_a = 1$ to $S_a = -1$. The sublattice b, during the cooling process, underwent a first-order phase transition from $S_b = 0.56$ (HS state) to $S_b = -0.79$ (LS state). At low temperatures, S_b reached a value of -1.

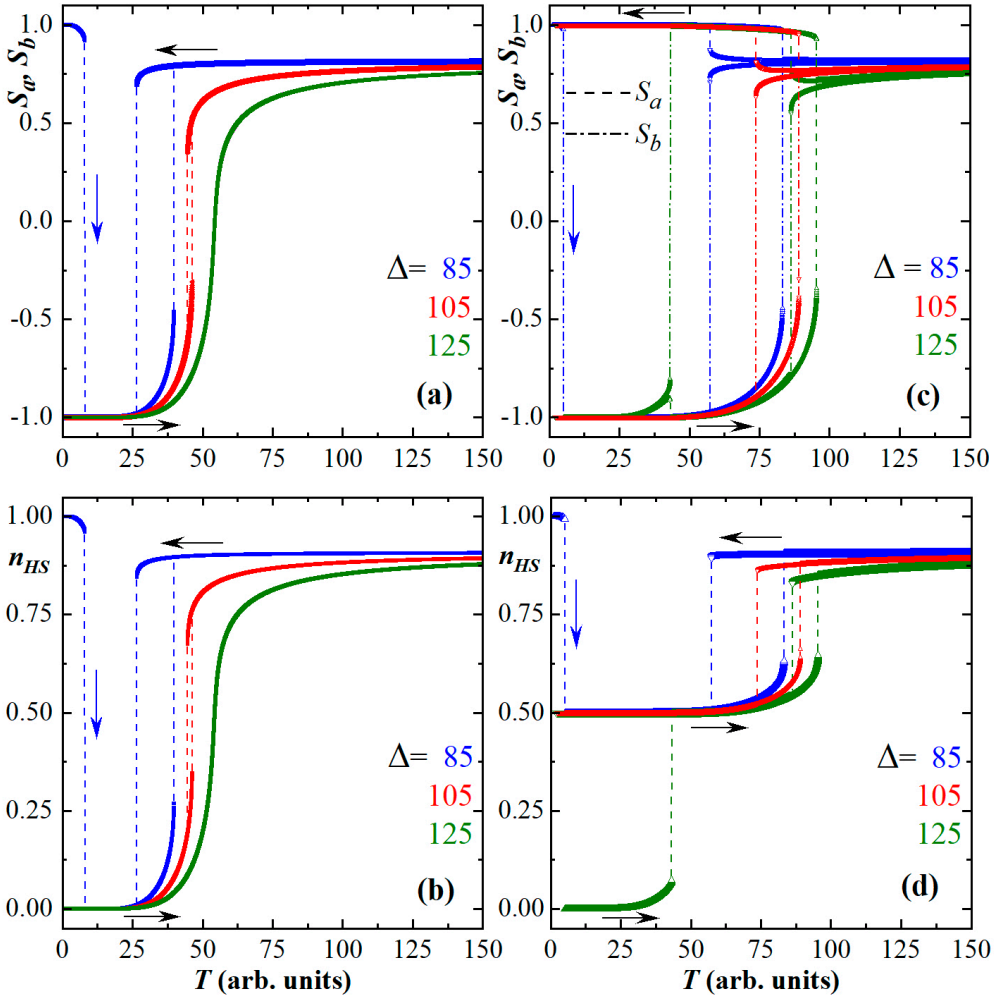


Figure 4. Thermal behaviors of the order parameters S_a, S_b, and high-spin fraction n_{HS} in the absence of the external magnetic field for different selected values of the ligand field parameter (Δ). In panels (**a**,**b**), $J_a = J_b = 50$, that is, the sublattices are equivalent, while, in panels (**c**,**d**), $J_a = 51$ and $J_b = 50$, that is, the sublattices are nonequivalent. Other parameters are the same: $J_{ab} = -50$, g = 10, and $H = 0.0$.

In Figure 4d, the temperature dependences of n_{HS} are shown. When $\Delta = 85$/blue curve and other parameter values matched those given in the figure caption, in the warming process, we found that the high-spin fraction n_{HS} displayed a stable HS state in the low temperature region and jumped to the intermediate metastable/stable state HS–LS at $n_{HS} = 0.5$. The study published by Gindulescu et al. [59] shows that compounds exhibiting a two-step thermal transition display a metastable state at low temperatures which cor-

responds to a high-spin fraction ($n_{HS} = 0.5$). At higher region temperatures, the thermal hysteresis was present separately from the stable HS state at low temperatures. For higher values of $\Delta(= 125)$, the stable state disappeared and a hidden LS state occurred. This state remained stable until $T = 43.8$, when the system transitioned from the LS state to the intermediate HS–LS state, leading to a two-step transition. The hidden spin state results align well with experimental findings obtained through the application of pressure or the light-induced excited spin state trapping process [28,60–63].

Figure 5 displays the magnetic field dependencies of S_a, S_b, and n_{HS} for various temperature values and specific values of the intrasublattice parameter. When $J_a = J_b = 50$, the sublattices are equivalent, while, when $J_a = 51$ and $J_b = 50$, the sublattices are nonequivalent. The other parameters were: $J_{ab} = -50$, g $= 10$, and $\Delta = 85$. In the case of equivalent sublattices, S_a, S_b, and n_{HS} exhibited a first-order transition at $T = 40$ when the external magnetic field was increased and decreased. The transition became gradual (smooth) at $T = 50$ and $T = 55$ (Figure 5a,b). The order parameters of the system exhibited a first-order transition with hysteresis and n_{HS} exhibited a two-step transition with hysteresis at temperatures of 40, 50, and 55 for nonequivalent sublattices (Figure 5c,d). Theoretical research has recently shown similarities in properties when examining the impact of an external magnetic field on SCO systems [64–66].

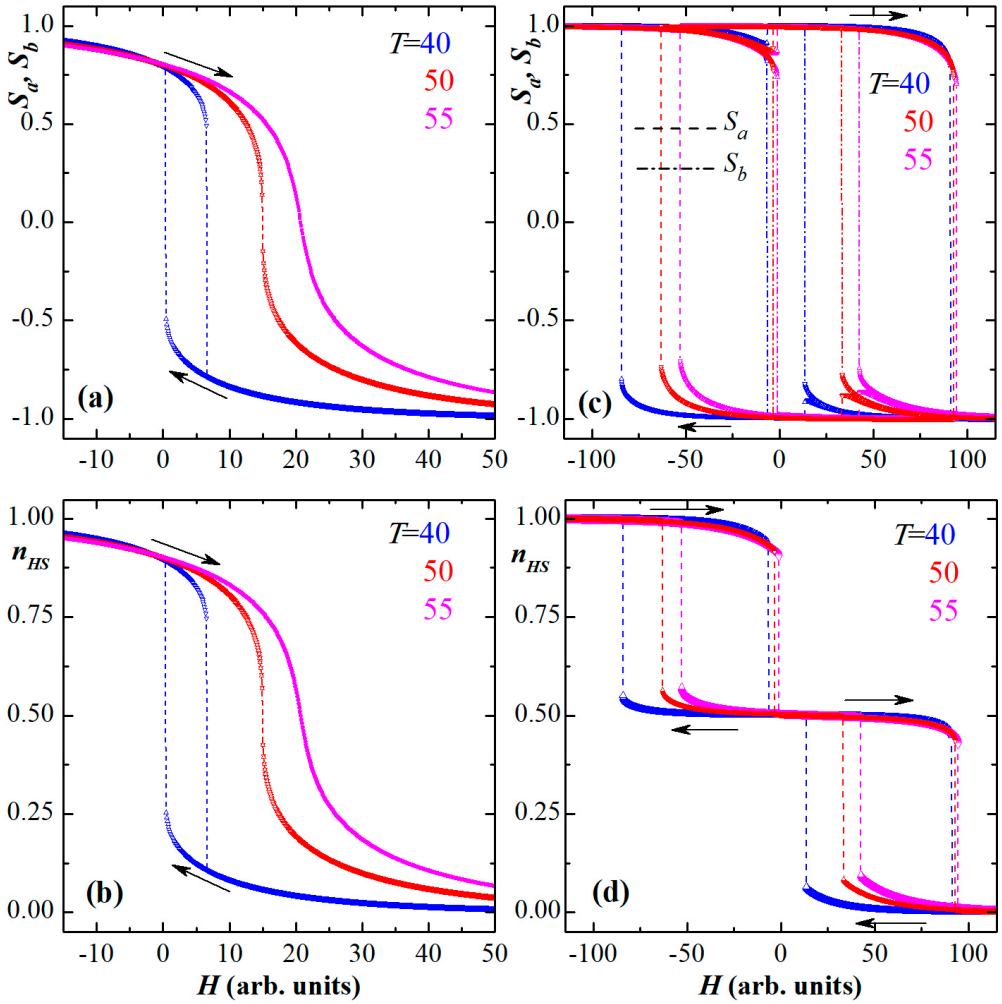


Figure 5. The external magnetic field evolution of the order parameters S_a, S_b, and high-spin fraction n_{HS} for different selected values of temperature (T). In panels (**a**,**b**), $J_a = J_b = 50$, that is, the sublattices are equivalent, while, in panels (**c**,**d**), $J_a = 51$ and $J_b = 50$, that is, the sublattices are nonequivalent. Other parameters are the same: $J_{ab} = -50$, g $= 10$, and $\Delta = 85$.

The final simulations for the static properties in this study concern the case where the difference between the intrasublattice parameters is very large, $J_a = 200$ and $J_b = 100$. We obtained the order parameters and high-spin fraction, which appear in Figure 6a,b. The other parameter values were: $J_{ab} = -50$, $\Delta = 900$, g $= 400$ and $H = 0.0$. Similar properties are depicted in Figure 1c,d. We obtained this separately to study the dynamic properties of S_a, S_b, and n_{HS}.

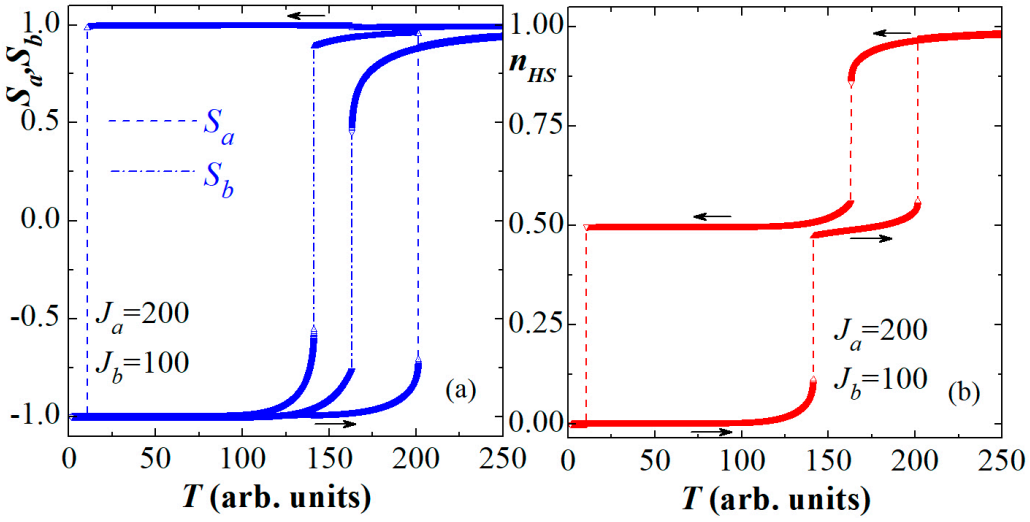


Figure 6. Thermal behaviors of the order parameters S_a and S_b (**a**) and high-spin fraction n_{HS} (**b**) in the absence of the external magnetic field. In panels (**a**,**b**): $J_a = 200$ and $J_b = 100$, that is, the sublattices are nonequivalent. Other parameters are: $J_{ab} = -50$, $\Delta = 900$, g $= 400$, and $H = 0.0$.

3.2. Time-Dependent Behaviors

Finally, we studied the dynamic properties of the system by solving Equation (13), which represent the equation of motion. Figure 7 presents the time evolution of the order parameters S_a, S_b, and n_{HS} at three different fixed temperatures: $T = 75$, 150, and 200. The equivalent sublattice parameters for this case were as follows: $J_a = J_b = 200$, $J_{ab} = -50$, $\Delta = 900$, g $= 400$, $k_1 = 1$, and $H = 0.0$. These parameters are identical to those shown in Figure 1a,b. Figure 7a,b display the relaxation of S_a, S_b, and n_{HS} for different initial values of the order parameters (-1 to $+1$ with a step of 0.25) below the hysteretic temperature ($T = 75$). The order parameters S_a, S_b, and n_{HS} evolved from the initial values to the stable state of the system. In the stable state, S_a and S_b had a value of -1 (LS), while n_{HS} had a value of 0 (LS). For the fixed temperature $T = 150$, the relaxation curves from different initial values of the order parameters were more complex. As shown in Figure 7c,d, the relaxation is characteristic of a typical bistable behavior. The S_a and S_b evolved in time from the initial values to one of the stable states -1 (LS) or $+1$ (HS). Similarly, the n_{HS} changed over time from the initial values to one of the stable states 0 (LS) or $+1$ (HS). At $T = 200$, the S_a, S_b, and n_{HS} saturated HS ($+1$) from the initial values, indicating that the system was in a stable state.

Figures 8 and 9 present the time dependence of the order parameters S_a, S_b, and n_{HS} at four different fixed temperatures: $T = 5$, 15, 35, and 125. Figures 8a and 9a show S_a, S_b, and n_{HS} at a fixed temperature of $T = 5$, which corresponds to the existence of the hidden stable state, and the system staying in the HS state for initial values of order parameters 0.9 and 1. The curves starting from the initial values of the order parameters $S_a = S_b \leq 0.8$ relaxed faster at the LS stable state for S_a, S_b, and n_{HS}. Similar bistability at low temperatures was observed previously by Enachescu et al. [67]. At a constant temperature of $T = 15$, which corresponds to a stable LS (low spin) state of the S_a, S_b, and n_{HS} order parameters, the relaxation curve exhibited a sigmoidal shape for higher initial values from the HS to the LS state. This can be observed in Figures 8b and 9b. As the

initial values of the order parameters decreased, the sigmoidal shape of the relaxation curve diminished. These properties are confirmed by the experimental results previously obtained for the $[Fe_{0.5}Zn_{0.5}(btr)_2(NCS)_2]H_2O$ compound [68], as well as by the experimental and theoretical results observed previously by Chakraboty et al. [69].

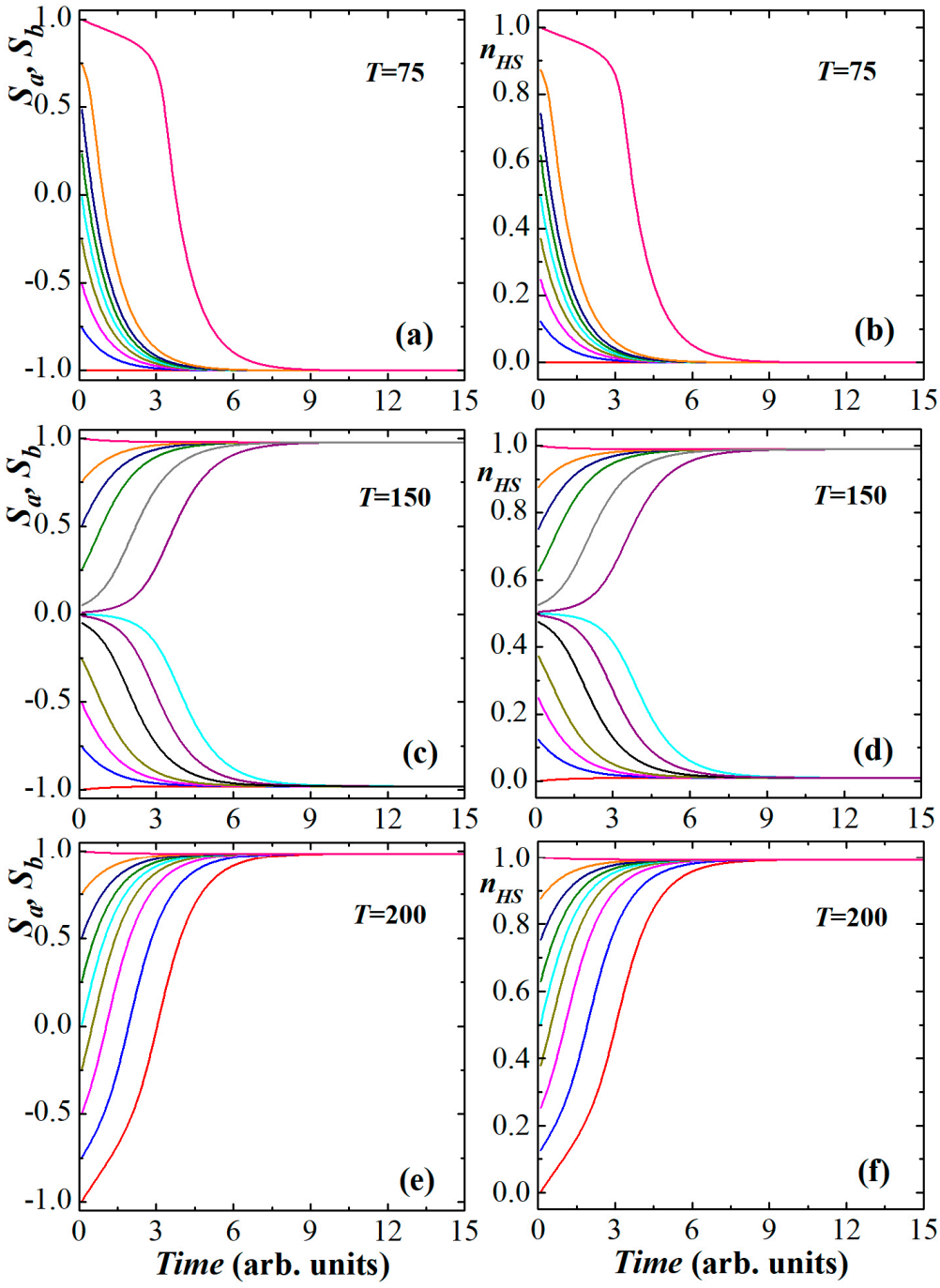


Figure 7. Relaxation curves of the order parameters S_a and S_b in panels (**a**,**c**,**e**) and of the high-spin fraction n_{HS} in panels (**b**,**d**,**f**) at various temperatures. These temperatures include those *below* the hysteretic temperature ($T = 75$), *above* the hysteretic temperature ($T = 200$), and within the bistability region ($T = 150$). The curves are plotted for different initial values of the order parameters S_a and S_b. Using the following parameter values: $J_a = J_b = 200$ (for equivalent sublattices, as shown in Figure 1a,b, $J_{ab} = -50$, $\Delta = 900$, g = 400, $k_1 = 1$, and $H = 0.0$).

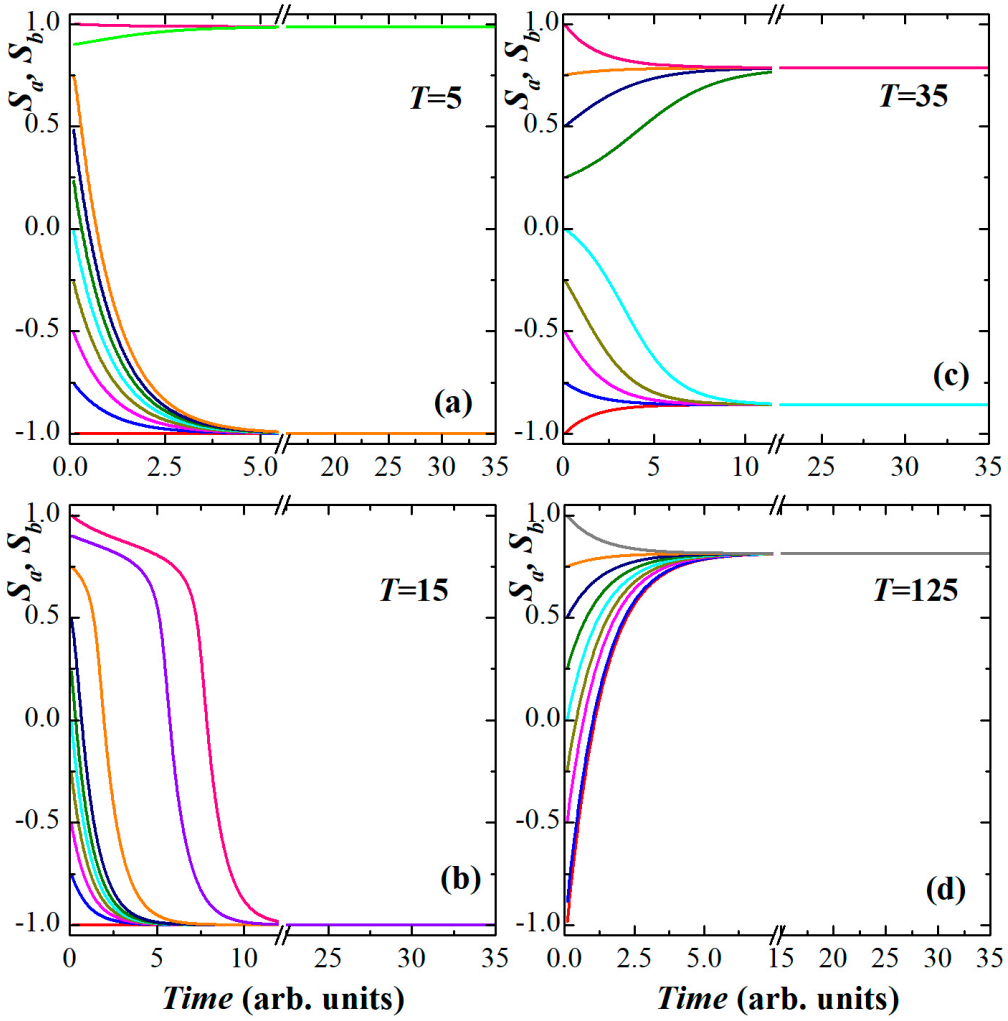


Figure 8. Relaxation curves of the order parameters S_a and S_b at various temperatures. These temperatures include those *below* the hysteretic low temperature stable state ($T = 5$) (**a**), *below* the hysteretic temperature ($T = 15$) (**b**), within the bistability region ($T = 35$) (**c**), and *above* the hysteretic temperature ($T = 125$) (**d**). The curves are plotted for different initial values of the order parameters S_a and S_b. Using the following parameter values: $J_a = 50$, $J_b = 50$ (representing equivalent sublattices, as shown in Figure 4a), $J_{ab} = -50$, $\Delta = 85$, g $= 10$, $k_1 = 1$, and $H = 0.0$.

The relaxation curves for different initial values of the order parameters at a temperature of $T = 35$, within the region where bistability occurs, are shown in Figures 8c and 9c. The specified system parameters ($J_a = J_b = 50$, $J_{ab} = -50$, $\Delta = 85$/blue curve, g $= 10$, $k_1 = 1$, and $H = 0.0$) in Figure 4a,b confirm the presence of thermal hysteresis around the transition temperature for the equivalent sublattices. The relaxation curves in this region converged toward either one of the two metastable/stable states, depending on the initial values of the order parameters.

That is strong evidence of bistable properties, a finding which has been confirmed by several theoretical and experimental studies [15,70,71]. At a constant temperature of $T = 125$, the system exhibits a stable state, which can be confirmed by the flow diagram.

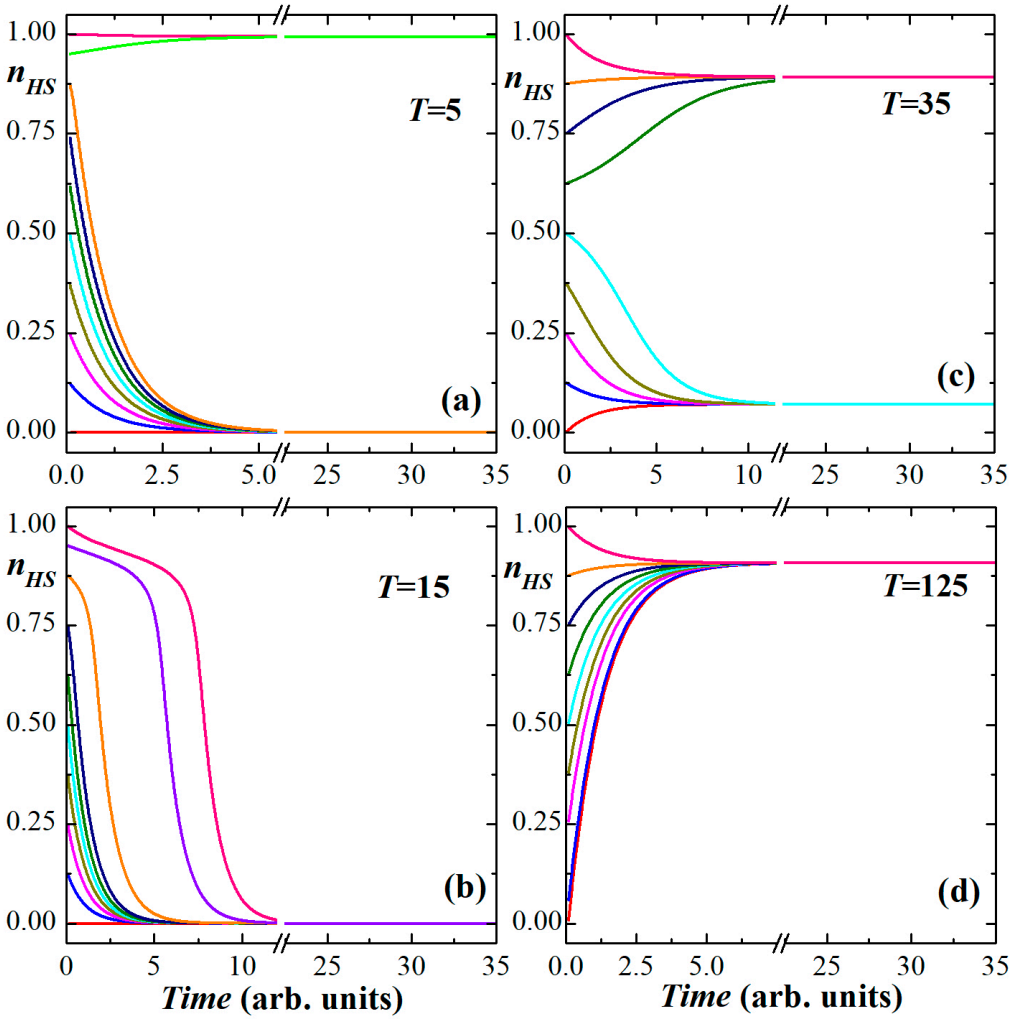


Figure 9. Relaxation curves of the high-spin fraction n_{HS} at various temperatures. These temperatures include those *below* the hysteretic low temperature stable state ($T = 5$) (**a**), *below* the hysteretic temperature ($T = 15$) (**b**), within the bistability region ($T = 35$) (**c**), and *above* the hysteretic temperature ($T = 125$) (**d**). The curves are plotted for different initial values of the order parameters S_a and S_b. Using the following parameter values: $J_a = 50$, $J_b = 50$ (representing equivalent sublattices, as shown in Figure 4b), $J_{ab} = -50$, $\Delta = 85$, g $= 10$, $k_1 = 1$, and $H = 0.0$.

In the previous figures, we assumed that the sublattices a and b were equivalent. However, we investigated the dynamic properties of nonequivalent sublattices, as shown in Figures 10 and 11. Different relaxation curves of the S_a and S_b for different initial values of the order parameters $S_a = S_b = 0.75,\ 0.9,\ 1$ were found at a fixed temperature $T = 5$, as shown in Figure 10a. The sublattice a represented by the order parameters S_a for these three selected values stayed in the HS (=1) steady state, whereas the sublattice b represented by the order parameters S_b relaxed in the LS (=1) steady state. For all the initial values of the order parameters $S_a = S_b < 0.75$, all the curves relaxed into the LS steady state. With respect to the high-spin fraction n_{HS} for the same conditions and for the initial values of the order parameters $S_a = S_b = 0.75,\ 0.9,\ 1$, the relaxation from HS converted and reached a plateau at about $n_{HS} = 0.5$, depicted in Figure 11a. At this plateau, as shown, the sublattices were in different spin states (HS–LS). For other initial values of the order parameters, the n_{HS} relaxation curve reached LS. At the constant temperature of $T = 35$ (Figure 10b), for the order parameters S_a and S_b, the relaxation curves transitioned $HS \leftrightarrow LS$ from different initial values of the order parameters. This typical bistability property of the order parameters corresponds to the nonequivalent intrasublattice parameters. The properties of S_a and S_b reported here are comparable with

experimental results for nonequivalent sublattices of the $[Fe(etz)_6](BF_4)_2$ spin-crossover system observed previously by Hinek et al. [72,73]. While all the relaxation curves of the high-spin fraction n_{HS} starting from different initial values (Figure 11b) converged to a stable state with a high-spin fraction $n_{HS} = 0.5$, the dynamic properties of the high-spin fraction matched the steady-state static properties shown in Figure 4c at the temperature of $T = 35$.

We obtained the relaxation curve in the bistable regions of S_a, S_b, and n_{HS} at a temperature of $T = 60$. The relaxation curves started with different initial values of the order parameters and relaxed into different, separated steady states, a phenomenon which is clear evidence of self-organization in the bistable region. Varret et al., during the experimental study of the HS fraction of $[Fe(ptz)_6](BF_4)_2$, presented the results for n_{HS} (starting values of 0.4 and 0.6) at a constant temperature which remained invariant during more than 5 h of irradiation [74]. The bistable state can be confirmed even for the high-spin fraction at this fixed temperature. In the high-temperature ($T = 100$) region, the relaxation curves from the initial values converged into the stable HS state. The selected value parameters for Figures 10 and 11 are the same as in Figure 4c for ligand field energy $\Delta = 85$.

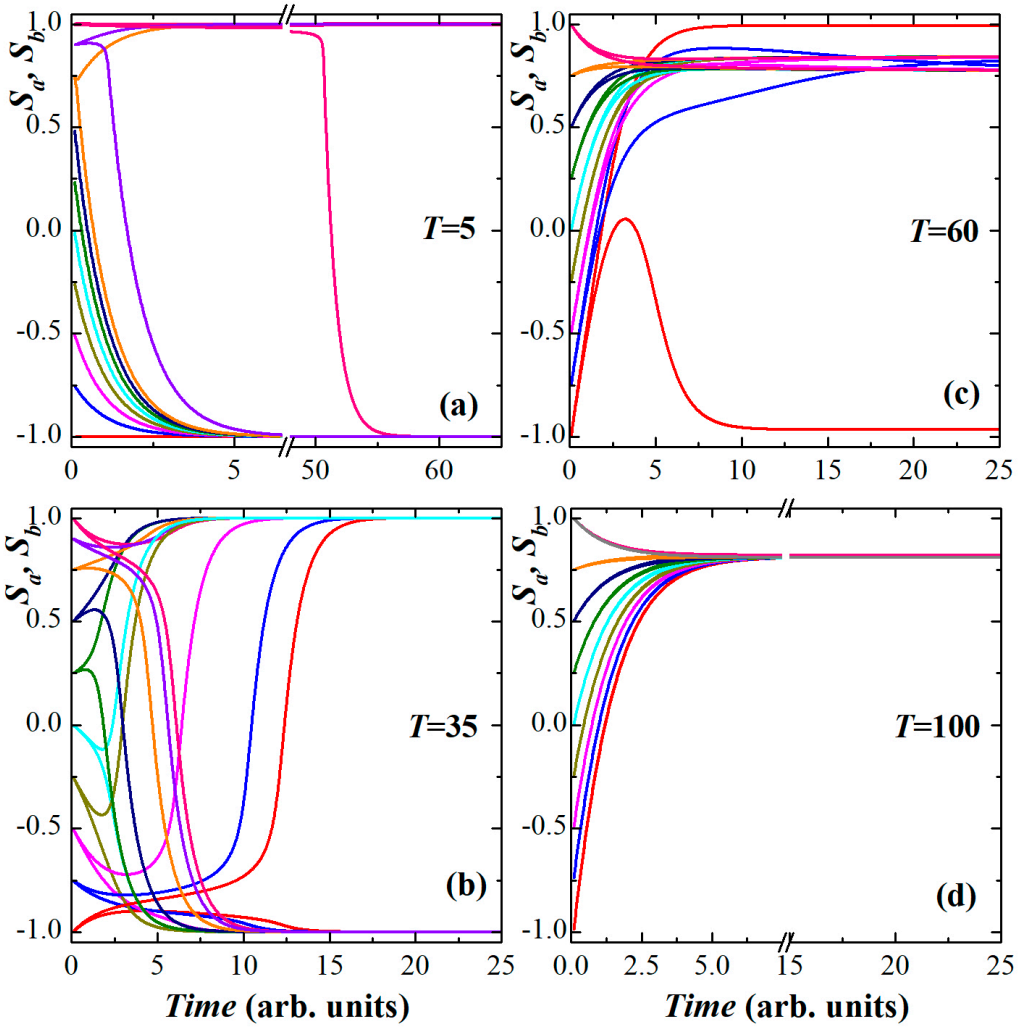


Figure 10. Relaxation curves of the order parameters S_a and S_b in the case of $J_a = 51$, $J_b = 50$ (representing nonequivalent sublattices, as shown in Figure 4c) at various temperatures. These temperatures include those *below* the hysteretic low temperature ($T = 5$) (**a**), *below* the hysteretic temperature ($T = 35$) (**b**), within the bistability region ($T = 60$) (**c**), and *above* the hysteretic temperature ($T = 100$) (**d**). Different initial values of the order parameters S_a and S_b are considered. Other parameters are the same values as in Figure 4c: $J_{ab} = -50$, $\Delta = 85$, g = 10, $k_1 = 1$, and $H = 0.0$.

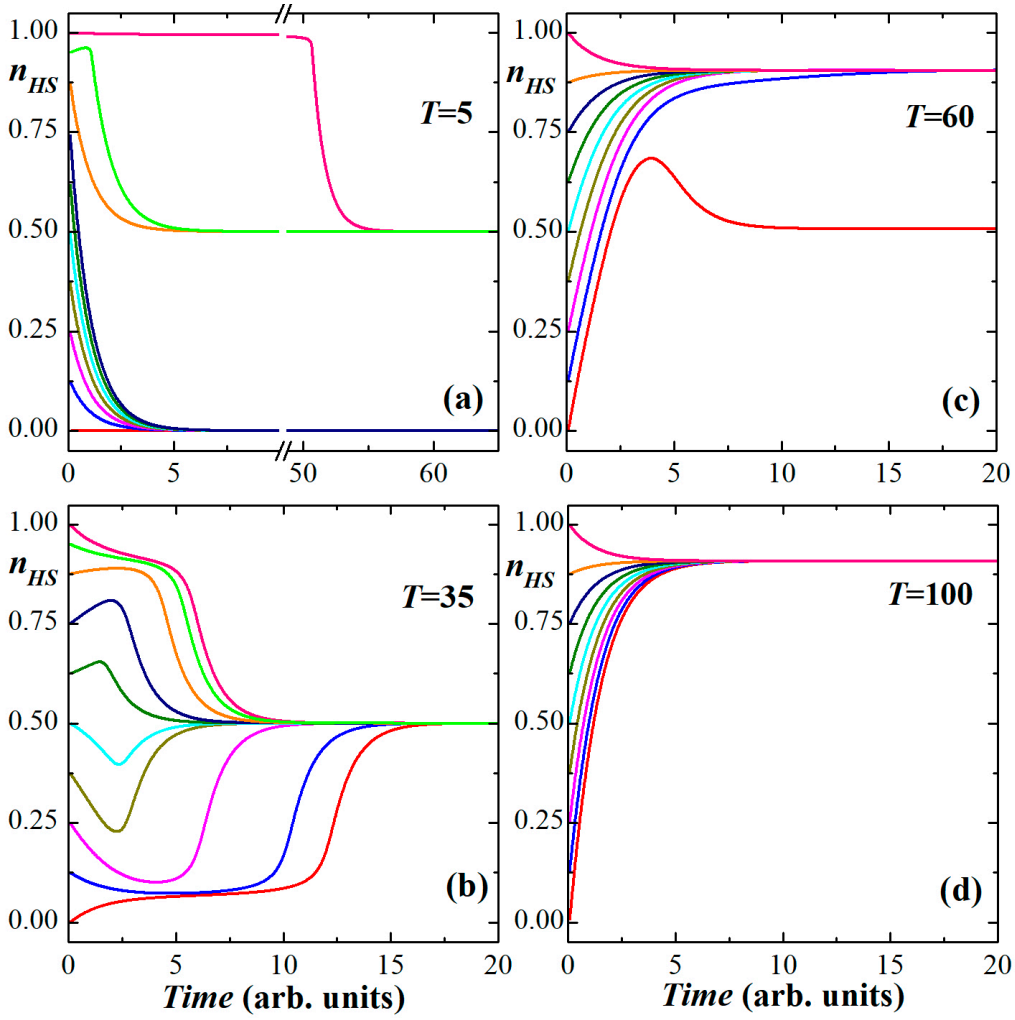


Figure 11. Relaxation curves of the high-spin fraction n_{HS} in the case of $J_a = 51$, $J_b = 50$ (representing non-equivalent sublattices, as shown in Figure 4c) at various temperatures. These temperatures include those *below* the hysteretic low temperature ($T = 5$) (**a**), *below* the hysteretic temperature ($T = 35$) (**b**), within the bistability region ($T = 60$) (**c**), and *above* the hysteretic temperature ($T = 100$) (**d**). Different initial values of the order parameters S_a and S_b are considered. Other parameters are the same values as in Figure 4c: $J_{ab} = -50$, $\Delta = 85$, g $= 10$, $k_1 = 1$, and $H = 0.0$.

We analyzed the dynamic properties of the system for nonequivalent sublattices in cases where the difference between the intrasublattice parameters was higher ($J_a = 200$ and $J_b = 100$), as shown in Figure 6 at the equilibrium property. Other parameters were: $J_{ab} = -50$, $\Delta = 900$, g $= 400$, $k_1 = 1$, and $H = 0.0$. As we reported before, S_a, S_b, and n_{HS} evolved from the initial values to the stable state of the system at a fixed temperature of $T = 5$. The values of S_a and S_b were both -1 (LS), while the value of n_{HS} was 0 (LS). At a temperature of $T = 125$, the order parameters S_a, S_b, and n_{HS} in the bistable region reached the following values during relaxation from different initial values: $S_a \simeq \pm 1$ for sublattice a, $S_b \simeq -0.92$ for sublattice b, and the high-spin fraction at $n_{HS} = 0.5$ and $n_{HS} = 0.02$. It is important to emphasize that the different initial values of the order parameters, e.g., $S_a = -0.5$ and $S_b = 0.5$ (curves with a violet color), exhibited a distinct relaxation pattern. The S_a relaxed more rapidly from its initial value to $S_a \simeq -1$, whereas the S_b relaxation process exhibited a two-step behavior with a sigmoidal nature until it reached $S_b \simeq -0.92$. The relaxation process of the high-spin fraction exhibited a two-step behavior with a sigmoidal nature, which is typical for nonlinear relaxation of cooperative origin [43], as presented in Figure 13b. The experiments [33] observed this form of relaxation.

At a temperature of $T = 150$, a bistable state was observed, as depicted in Figure 12c. The order parameters of sublattice a and b both reached a steady state with values of $S_a \simeq \pm 1$ and $S_b \simeq \pm 0.91$, respectively. The relaxation of the high-spin fraction took place at two separate steady states, with $n_{HS} = 0.52$ and $n_{HS} = 0.48$, depending on the initial values of the order parameters. The nonequilibrium properties corresponded with the static properties observed at the separate branches in the plateau region between the hysteresis loop during both the warming and cooling processes, as depicted in Figure 6b. The order parameters S_a, S_b, and n_{HS}, depicted in Figures 12d and 13d, were obtained at a constant temperature of $T = 225$. These order parameters were relaxed from various initial values and reached the HS state.

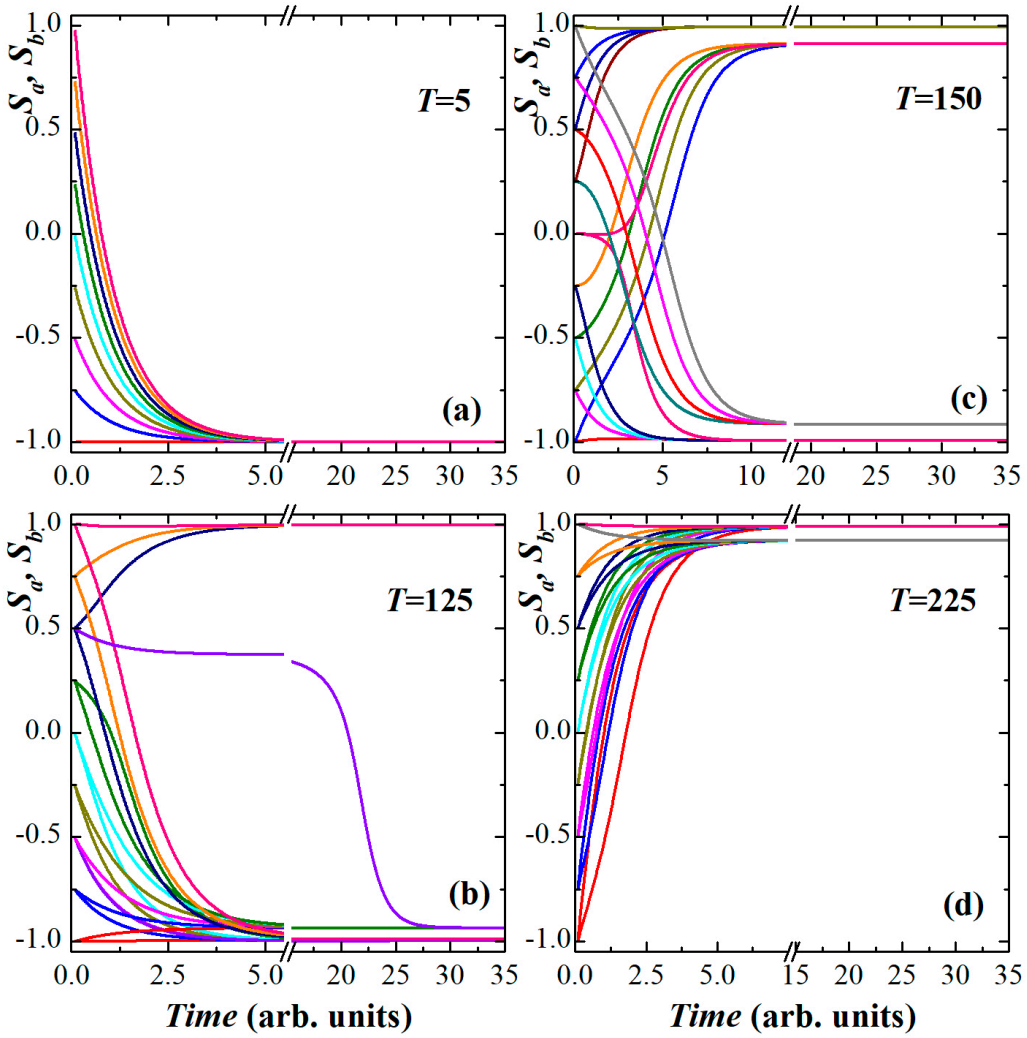


Figure 12. Relaxation curves of the order parameters S_a, S_b *below* the hysteretic temperature ($T = 5$) (**a**), in the *bistability* ($T = 125$, 150) region panels (**b**,**c**), and *above* the hysteretic temperature ($T = 225$) (**d**), for different initial values of the order parameters S_a and S_b. With the parameter values: $J_a = 200$, $J_b = 100$ (nonequivalent sublattices, Figure 6a), $J_{ab} = -50$, $\Delta = 900$, g $= 400$, $k_1 = 1$, and $H = 0.0$.

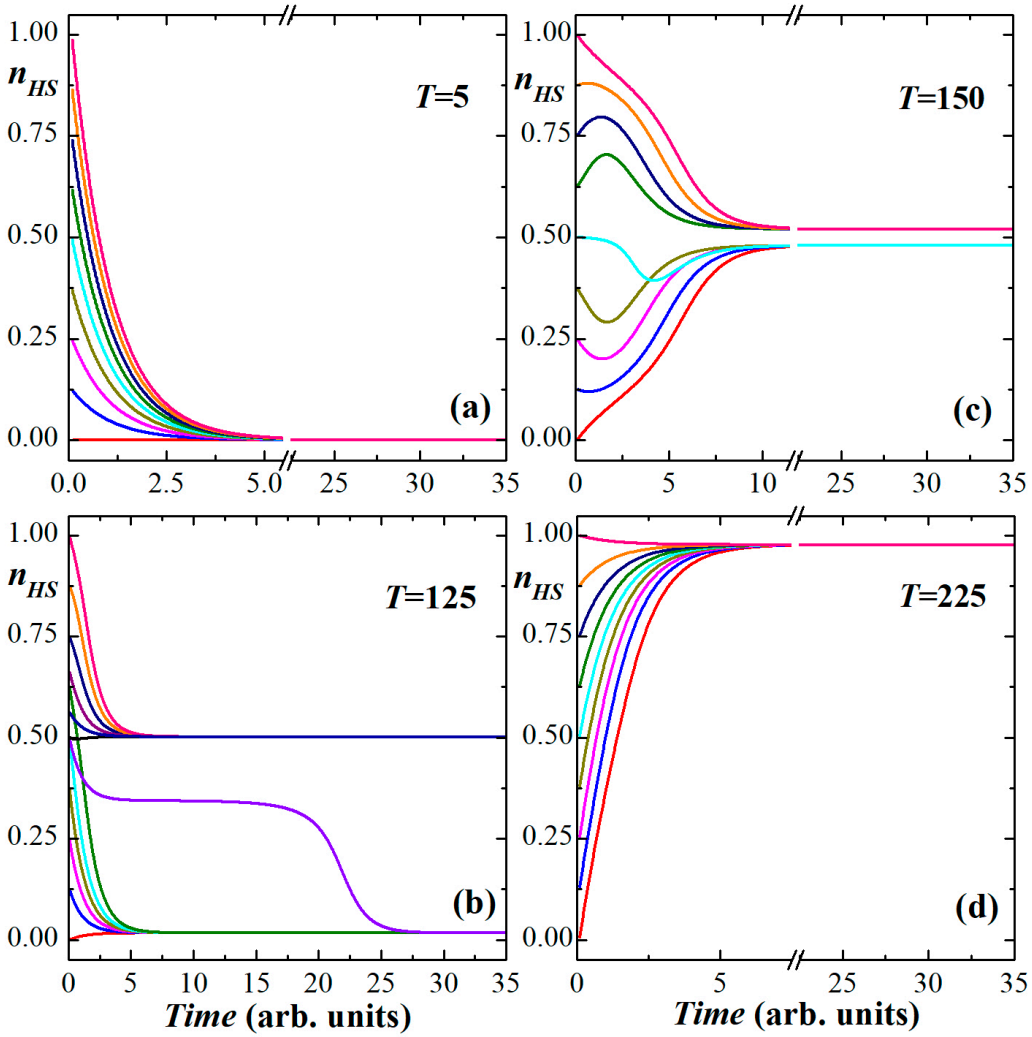


Figure 13. Relaxation curves of the high-spin fraction n_{HS} (**a**) *below* the hysteretic temperature ($T = 5$), (**b**) in the *bistability* ($T = 125$) region, (**c**) in the *flat* ($T = 150$) region of the two-step spin-crossover system, and (**d**) *above* the hysteretic temperature ($T = 225$) for different initial values of the order parameters S_a, S_b. With the parameter values: $J_a = 200$, $J_b = 100$ (nonequivalent sublattices, Figure 6b), $J_{ab} = -50$, $\Delta = 900$, g = 400, $k_1 = 1$, and $H = 0.0$.

The above relaxation results can also be observed using the flow diagrams in a two-dimensional $S_a - S_b$ phase space describing the solutions of the dynamic equation. The flow diagram of S_a and S_b are presented for the rate constant $k_1 = 1$ and for different temperatures in Figures 14 and 15, respectively. The flow diagrams of the order parameters S_a and S_b for equivalent sublattices are shown in Figure 14a–d, under a constant temperature (T = 5, 15, 35, and 125); all other parameters correspond to the situations in Figures 4a and 8. The open circle represents the stable equilibrium solution, which corresponds to the lowest values of the free energy or the deepest minimum. On the other hand, the filled circle represents the unstable solution or state, which corresponds to local maxima (the peaks) or a saddle point in these figures.

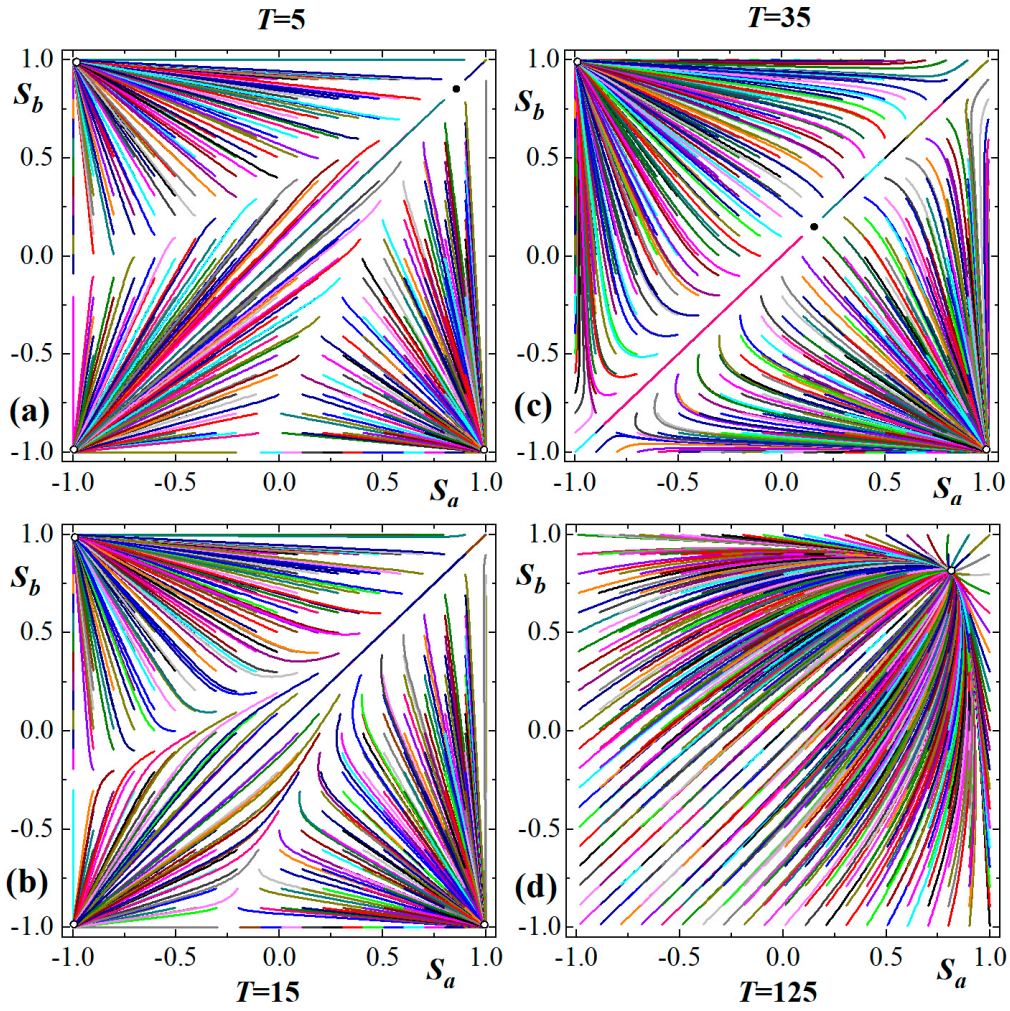


Figure 14. Flow diagram of the system for order parameters S_a and S_b with different temperature values. (**a**) for $T = 5$, (**b**) for $T = 15$, (**c**) for $T = 35$, and (**d**) for $T = 125$, with other parameter values: $J_a = 50$, $J_b = 50$ (equivalent sublattices, Figures 4a and 8), $J_{ab} = -50$, $\Delta = 85$, g = 10, $k_1 = 1$, and $H = 0.0$. The filled circle corresponds to the unstable state and the open circle corresponds to the stable state.

The flow diagrams of the order parameters S_a and S_b for nonequivalent sublattices are shown in Figure 15a–d, under a constant temperature (T = 5, 35, 60, and 100); all other parameters correspond to the situations in Figures 4c and 10. In addition, in Figure 15, the open circle represents the stable equilibrium state, whereas the filled circle represents the unstable state. Moreover, the filled square depicted in Figure 15c represents the metastable state. This state is reached when the system relaxes into it, but it does not correspond to the deepest minimum. Instead, it corresponds to a secondary minimum. The nonlinear differential equation (Equation (13)) can be numerically solved using the Runge–Kutta method.

Consequently, with these dynamic studies and the flow diagrams of S_a and S_b, we verified the stable, metastable, and unstable branches of the order parameters and high-spin fraction that we had found in the equilibrium study.

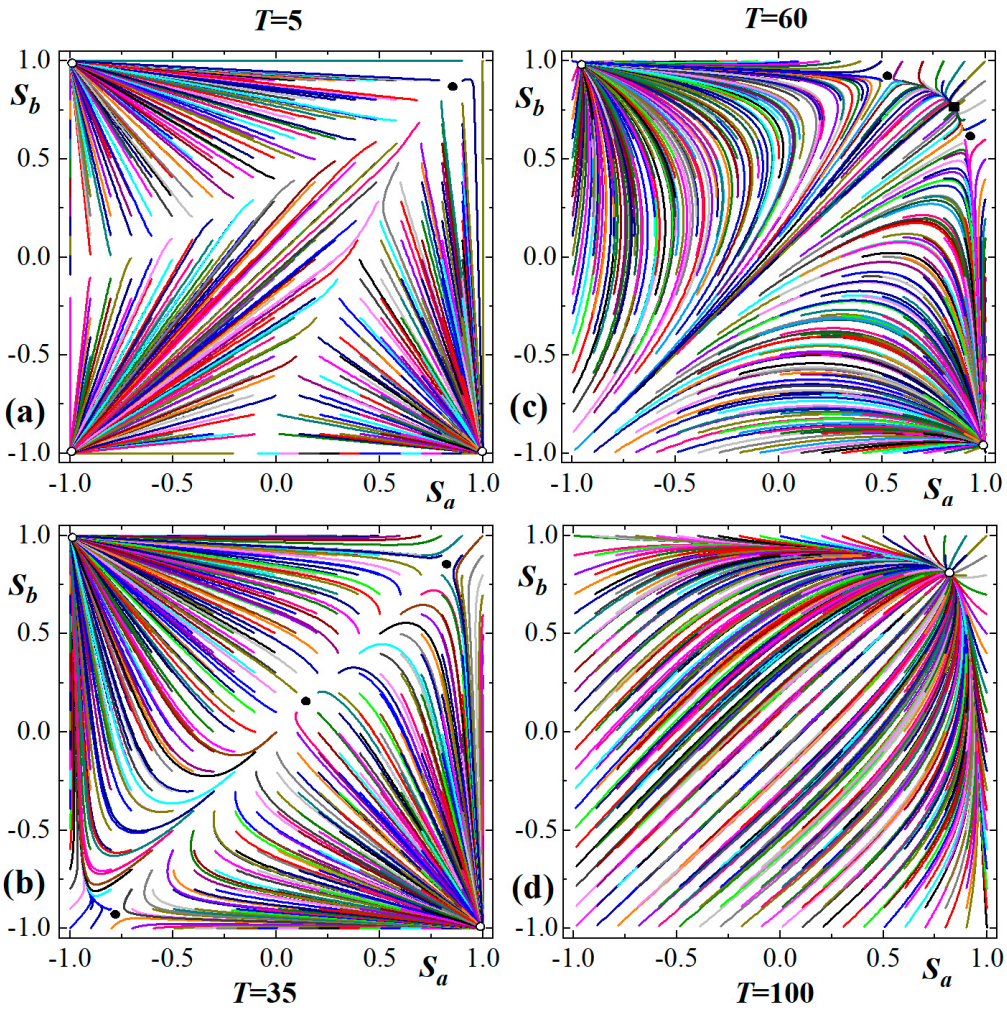


Figure 15. Flow diagram of the system for order parameters S_a and S_b with different temperature values. (**a**) for $T = 5$, (**b**) for $T = 35$, (**c**) for $T = 60$, and (**d**) for $T = 100$, with other parameter values: $J_a = 51$, $J_b = 50$ (nonequivalent sublattices, Figures 4c and 10), $J_{ab} = -50, \Delta = 85$, g = 10, $k_1 = 1$, and $H = 0.0$. The filled circle corresponds to the unstable state, the filled square corresponds to the metastable state, and the open circle corresponds to the stable state.

4. Conclusions

We used the lowest approximation of the cluster variation method and the path probability method to analyze the equilibrium and nonequilibrium properties of the order parameters S_a, S_b, and high-spin fraction n_{HS} in the spin-crossover system of the two-sublattice model. Equivalent and nonequivalent sublattices were considered for the presented model. The main focus of the study is on how the intersublattice parameter, intrasublattice parameter, degeneracy, ligand field energy, and external magnetic field affect the phase transition properties of the spin-crossover system. The SCO system exhibited gradual and first-order phase transitions with varying values of the model parameters. For nonequivalent sublattices, the order parameters had an intermediate temperature, where sublattices have different states for specific values of the antiferromagnetic ($J_{ab} < 0$) intersublattice interaction. The high-spin fraction n_{HS} exhibited a first-order phase transition with two-step properties and a plateau region between the hysteresis loop during both the warming and cooling processes. In addition, we show the presence of a stable high-spin state of n_{HS} at a low temperature for both equivalent and nonequivalent sublattices. It is noteworthy that, for the first time for nonequivalent sublattices, we observed a transition from the stable high-spin state to the intermediate stable HS–LS state at a value of $n_{HS} = 0.5$ in the low temperature region. The dynamic properties were observed. The phenomenon

of bistability occurred at low temperatures. The relaxation curves started with different initial values of the order parameters and relaxed into different, separated steady states, a phenomenon which is clear evidence of self-organization in the bistable region. It is important to emphasize that, for the different initial values of the order parameters, the relaxation process of the order parameters and the high-spin fraction exhibited a two-step behavior with a sigmoidal nature. With these dynamic studies and the flow diagrams of S_a and S_b, we also verified the existence of the stable, metastable, and unstable branches of the order parameters and high-spin fraction that have been found in some earlier equilibrium studies [75,76].

Author Contributions: Conceptualization, V.V.; methodology, V.V., O.Y. and R.E.; software, V.V. and O.Y.; validation, V.V., O.Y., S.Ö. and R.E.; formal analysis, V.V., O.Y., S.Ö. and R.E.; investigation, O.Y., S.Ö. and R.E.; writing—original draft preparation, V.V.; visualization, V.V. All authors have read and agreed to the published version of the manuscript.

Funding: This research received no external funding.

Institutional Review Board Statement: Not applicable.

Informed Consent Statement: Not applicable.

Data Availability Statement: The original contributions presented in the study are included in the article, further inquiries can be directed to the corresponding author.

Conflicts of Interest: The authors declare no conflicts of interest.

References

1. Gütlich, P.; Gaspar, A.B.; Garcia, Y. Spin state switching in iron coordination compounds. *Beilstein J. Org. Chem.* **2013**, *9*, 342–391. [CrossRef]
2. Bousseksou, A.; Molnár, G.; Salmon, L.; Nicolazzi, W. Molecular spin crossover phenomenon: Recent achievements and prospects. *Chem. Soc. Rev.* **2011**, *40*, 3313–3335. [CrossRef]
3. Lefter, C.; Tan, R.; Tricard, S.; Dugay, J.; Molnár, G.; Salmon, L.; Carrey, J.; Rotaru, A.; Bousseksou, A. On the stability of spin crossover materials: From bulk samples to electronic devices. *Polyhedron* **2015**, *102*, 434–440. [CrossRef]
4. Kahn, O.; Martinez, C.J. Spin-Transition Polymers: From Molecular Materials Toward Memory Devices. *Science* **1998**, *279*, 44–48. [CrossRef]
5. Von Ranke, P.; Alho, B.; Ribeiro, P. First indirect experimental evidence and theoretical discussion of giant refrigeration capacity through the reversible pressure induced spin-crossover phase transition. *J. Alloys Compd.* **2018**, *749*, 556–560. [CrossRef]
6. Gaspar, A.B.; Molnár, G.; Rotaru, A.; Shepherd, H.J. Pressure effect investigations on spin-crossover coordination compounds. *Comptes Rendus Chim.* **2018**, *21*, 1095–1120. [CrossRef]
7. Babilotte, K.; Boukheddaden, K. Theoretical investigations on the pressure effects in spin-crossover materials: Reentrant phase transitions and other behavior. *Phys. Rev. B* **2020**, *101*, 174113. [CrossRef]
8. Muñoz, M.C.; Real, J.A. Thermo-, piezo-, photo- and chemo-switchable spin crossover iron(II)-metallocyanate based coordination polymers. *Coord. Chem. Rev.* **2011**, *255*, 2068–2093. [CrossRef]
9. Bonnet, S.; Molnár, G.; Costa, J.S.; Siegler, M.A.; Spek, A.L.; Bousseksou, A.; Fu, W.-T.; Gamez, P.; Reedijk, J. Influence of Sample Preparation, Temperature, Light, and Pressure on the Two-Step Spin Crossover Mononuclear Compound [Fe(bapbpy)$(NCS)_2$]. *Chem. Mater.* **2009**, *21*, 1123–1136. [CrossRef]
10. Her, J.L.; Matsuda, Y.H.; Nakano, M.; Niwa, Y.; Inada, Y. Magnetic field-induced spin-crossover transition in [MnIII(taa)] studied by X-ray absorption spectroscopy. *J. Appl. Phys.* **2012**, *111*, 053921. [CrossRef]
11. Kimura, S.; Narumi, Y.; Kindo, K.; Nakano, M.; Matsubayashi, G.-E. Field-induced spin-crossover transition of [MnIII(taa)] studied under pulsed magnetic fields. *Phys. Rev. B* **2005**, *72*, 064448. [CrossRef]
12. Mahfoud, T.; Molnár, G.; Bonhommeau, S.; Cobo, S.; Salmon, L.; Demont, P.; Tokoro, H.; Ohkoshi, S.-I.; Boukheddaden, K.; Bousseksou, A. Electric-Field-Induced Charge-Transfer Phase Transition: A Promising Approach Toward Electrically Switchable Devices. *J. Am. Chem. Soc.* **2009**, *131*, 15049–15054. [CrossRef]
13. Lefter, C.; Tan, R.; Dugay, J.; Tricard, S.; Molnár, G.; Salmon, L.; Carrey, J.; Nicolazzi, W.; Rotaru, A.; Bousseksou, A. Unidirectional electric field-induced spin-state switching in spin crossover based microelectronic devices. *Chem. Phys. Lett.* **2016**, *644*, 138–141. [CrossRef]
14. Bonhommeau, S.; Molnár, G.; Goiran, M.; Boukheddaden, K.; Bousseksou, A. Unified dynamical description of pulsed magnetic field and pressure effects on the spin crossover phenomenon. *Phys. Rev. B* **2006**, *74*, 064424. [CrossRef]
15. Desaix, A.; Roubeau, O.; Jeftic, J.; Haasnoot, J.; Boukheddaden, K.; Codjovi, E.; Linarès, J.; Noguès, M.; Varret, F. Light-induced bistability in spin transition solids leading to thermal and optical hysteresis. *Eur. Phys. J. B* **1998**, *6*, 183–193. [CrossRef]

16. Stoleriu, L.; Chakraborty, P.; Hauser, A.; Stancu, A.; Enachescu, C. Thermal hysteresis in spin-crossover compounds studied within the mechanoelastic model and its potential application to nanoparticles. *Phys. Rev. B* **2011**, *84*, 134102. [CrossRef]
17. Paez-Espejo, M.; Sy, M.; Boukheddaden, K. Unprecedented Bistability in Spin-Crossover Solids Based on the Retroaction of the High Spin Low-Spin Interface with the Crystal Bending. *J. Am. Chem. Soc.* **2018**, *140*, 11954–11964. [CrossRef]
18. Gütlich, P. Spin crossover in iron(II)-complexes. *Struct. Bond.* **1981**, *44*, 83–195. [CrossRef]
19. König, E. Nature and dynamics of the spin-state interconversion in metal complexes. *Struct. Bond.* **1991**, *76*, 51–152. [CrossRef]
20. Kahn, O. Spin-crossover molecular materials. *Curr. Opin. Solid State Mater. Sci.* **1996**, *1*, 547–554. [CrossRef]
21. Gütlich, P.; Hauser, A.; Spiering, H. Thermal and Optical Switching of Iron(II) Complexes. *Angew. Chem. Int. Ed.* **1994**, *33*, 2024–2054. [CrossRef]
22. Decurtins, S.; Gütlich, P.; Köhler, C.; Spiering, H.; Hauser, A. Light-induced excited spin state trapping in a transition-metal complex: The hexa-1-propyltetrazole-iron (II) tetrafluoroborate spin-crossover system. *Chem. Phys. Lett.* **1984**, *105*, 1–4. [CrossRef]
23. Renz, F.; Spiering, H.; Goodwin, H.; Gütlich, P. Light-perturbed hysteresis in an iron(II) spin-crossover compound observed by the Mössbauer effect. *Hyperfine Interact.* **2000**, *126*, 155–158. [CrossRef]
24. Tayagaki, T.; Tanaka, K. Photoinduced Phase Transition to a New Macroscopic Spin-Crossover-Complex Phase. *Phys. Rev. Lett.* **2001**, *86*, 2886–2889. [CrossRef]
25. Freysz, E.; Montant, S.; Létard, S.; Létard, J.-F. Single laser pulse induces spin state transition within the hysteresis loop of an Iron compound. *Chem. Phys. Lett.* **2004**, *394*, 318–323. [CrossRef]
26. Bonhommeau, S.; Molnár, G.; Galet, A.; Zwick, A.; Real, J.; McGarvey, J.J.; Bousseksou, A. One Shot Laser Pulse Induced Reversible Spin Transition in the Spin-Crossover Complex $[Fe(C_4H_4N_2)\{Pt(CN)_4\}]$ at Room Temperature. *Angew. Chem.* **2005**, *117*, 4137–4141. [CrossRef]
27. Gudyma, I.; Maksymov, A.; Dimian, M. Stochastic kinetics of photoinduced phase transitions in spin-crossover solids. *Phys. Rev. E* **2013**, *88*, 042111. [CrossRef]
28. Milin, E.; Patinec, V.; Triki, S.; Bendeif, E.-E.; Pillet, S.; Marchivie, M.; Chastanet, G.; Boukheddaden, K. Elastic Frustration Triggering Photoinduced Hidden Hysteresis and Multistability in a Two-Dimensional Photoswitchable Hofmann-Like Spin-Crossover Metal–Organic Framework. *Inorg. Chem.* **2016**, *55*, 11652–11661. [CrossRef]
29. Kambara, T. Theory of Pressure-Induced High-Spin $\rightleftarrows$ Low-Spin Transition in Compounds of Iron. *J. Phys. Soc. Jpn.* **1981**, *50*, 2257–2264. [CrossRef]
30. Konishi, Y.; Tokoro, H.; Nishino, M.; Miyashita, S. Monte Carlo Simulation of Pressure-Induced Phase Transitions in Spin-Crossover Materials. *Phys. Rev. Lett.* **2008**, *100*, 067206. [CrossRef]
31. Shepherd, H.J.; Rosa, P.; Vendier, L.; Casati, N.; Létard, J.-F.; Bousseksou, A.; Guionneau, P.; Molnár, G. High-pressure spin-crossover in a dinuclear Fe(ii) complex. *Phys. Chem. Chem. Phys.* **2012**, *14*, 5265–5271. [CrossRef]
32. Bousseksou, A.; Nasser, J.; Linares, J.; Boukheddaden, K.; Varret, F. Ising-like model for the two-step spin-crossover. *J. Phys. I* **1992**, *2*, 1381–1403. [CrossRef]
33. Boukheddaden, K.; Linares, J.; Codjovi, E.; Varret, F.; Niel, V.; Real, J.A. Dynamical Ising-like model for the two-step spin-crossover systems. *J. Appl. Phys.* **2003**, *93*, 7103–7105. [CrossRef]
34. Bousseksou, A.; Varret, F.; Nasser, J. Ising-like model for the two step spin-crossover of binuclear molecules. *J. Phys. I* **1993**, *3*, 1463–1473. [CrossRef]
35. Hôo, B.; Boukheddaden, K.; Varret, F. Two-variable macroscopic model for spin-crossover solids: Static and dynamic effects of the correlations. *Eur. Phys. J. B* **2000**, *17*, 449–457. [CrossRef]
36. Nishino, M.; Miyashita, S. Dynamical process for switching between the metastable ordered magnetic state and the nonmagnetic ground state in a photoinduced phase transition. *Phys. Rev. B* **2001**, *63*, 174404. [CrossRef]
37. Boukheddaden, K.; Linares, J.; Spiering, H.; Varret, F. One-dimensional Ising-like systems: An analytical investigation of the static and dynamic properties, applied to spin-crossover relaxation. *Eur. Phys. J. B* **2000**, *15*, 317–326. [CrossRef]
38. Boukheddaden, K.; Varret, F.; Salunke, S.; Linares, J.; Codjovi, E. Non-linear Relaxation of the Photo-induced High Spin State in Spin-Crossover Solids: Effect of Correlations. *Phase Transit.* **2002**, *75*, 733–741. [CrossRef]
39. Boukheddaden, K.; Nishino, M.; Miyashita, S.; Varret, F. Unified theoretical description of the thermodynamical properties of spin crossover with magnetic interactions. *Phys. Rev. B* **2005**, *72*, 014467. [CrossRef]
40. Nasser, J. First order high-spin/low-spin phase transition induced by acoustic-phonons. *Eur. Phys. J. B* **2001**, *21*, 3–10. [CrossRef]
41. Mouri, S.; Tanaka, K.; Bonhommeau, S.; Moussa, N.O.; Molnár, G.; Bousseksou, A. Relaxation process from photoinduced states of double-step spin-crossover systems using a kinetic two-sublattice Ising-like model including intra-site coupling. *Phys. Rev. B* **2008**, *78*, 174308. [CrossRef]
42. Bousseksou, A.; Constant-Machado, H.; Varret, F. A Simple Ising-Like Model for Spin Conversion Including Molecular Vibrations. *J. Phys. I* **1995**, *5*, 747–760. [CrossRef]
43. Boukheddaden, K.; Shteto, I.; Hôo, B.; Varret, F. Dynamical model for spin-crossover solids. I. Relaxation effects in the mean-field approach. *Phys. Rev. B* **2000**, *62*, 14796–14805. [CrossRef]
44. Boukheddaden, K.; Shteto, I.; Hôo, B.; Varret, F. Dynamical model for spin-crossover solids. II. Static and dynamic effects of light in the mean-field approach. *Phys. Rev. B* **2000**, *62*, 14806–14817. [CrossRef]
45. Nishino, M.; Boukheddaden, K.; Miyashita, S.; Varret, F. Dynamical properties of photoinduced magnetism and spin-crossover phenomena in Prussian blue analogs. *J. Phys. Conf. Ser.* **2005**, *21*, 61–66. [CrossRef]

46. Boukheddaden, K.; Linares, J.; Tanasa, R.; Chong, C. Theoretical investigations on an axial next nearest neighbour Ising-like model for spin crossover solids: One- and two-step spin transitions. *J. Phys. Condens. Matter* **2007**, *19*, 106201. [CrossRef]
47. Nishino, M.; Yamaguchi, K.; Miyashita, S. Switching dynamics between the metastable ordered magnetic state and a nonmagnetic ground state: A possible mechanism for photoinduced ferromagnetism. *Phys. Rev. B* **1998**, *58*, 9303–9311. [CrossRef]
48. Bousseksou, A.; Nasser, J.; Varret, F. Specific heat of two-step spin conversions. *J. Magn. Magn. Mater.* **1995**, *140–144*, 1511–1512. [CrossRef]
49. Yalçın, O.; Veliu, V.; Özüm, S.; Erdem, R. Static and dynamic properties of two-sublattice spin-crossover systems. *Phys. B Condens. Matter* **2022**, *645*, 414230. [CrossRef]
50. Kikuchi, R. A Theory of Cooperative Phenomena. *Phys. Rev. B* **1951**, *81*, 988–1003. [CrossRef]
51. Kikuchi, R. The Path Probability Method. *Prog. Theor. Phys. Suppl.* **1966**, *35*, 1–64. [CrossRef]
52. Nishino, M.; Boukheddaden, K.; Miyashita, S.; Varret, F. Relaxation dynamics of two-step spin-crossover. *Polyhedron* **2005**, *24*, 2852–2856. [CrossRef]
53. Boča, R.; Linert, W. Is There a Need for New Models of the Spin Crossover? In *Molecular Magnets Recent Highlights*; Springer: Vienna, Austria, 2002; pp. 83–100. [CrossRef]
54. Boinnard, D.; Bousseksou, A.; Dworkin, A.; Savariault, J.M.; Varret, F.; Tuchagues, J.P. Two-step spin conversion of [FeII(5-NO2-sal-N(1,4,7,10))]: 292, 153, and 103 K X-ray crystal and molecular structure, infrared, magnetic, Moessbauer, calorimetric, and theoretical studies. *Inorg. Chem.* **1994**, *33*, 271–281. [CrossRef]
55. Nishino, M.; Boukheddaden, K.; Miyashita, S.; Varret, F. Arrhenius Monte Carlo study of two-step spin crossover: Equilibrium and relaxation paths. *Phys. Rev. B* **2003**, *68*, 224402. [CrossRef]
56. Miyashita, S.; Konishi, Y.; Tokoro, H.; Nishino, M.; Boukheddaden, K.; Varret, F. Structures of Metastable States in Phase Transitions with a High-Spin Low-Spin Degree of Freedom. *Prog. Theor. Phys.* **2005**, *114*, 719–735. [CrossRef]
57. Tokoro, H.; Miyashita, S.; Hashimoto, K.; Ohkoshi, S.-I. Huge thermal hysteresis loop and a hidden stable phase in a charge-transfer phase transition of $Rb_{0.64}Mn[Fe(CN)_6]_{0.88}\cdot 1.7H_2O$. *Phys. Rev. B* **2006**, *73*, 172415. [CrossRef]
58. Konishi, Y.; Tokoro, H.; Nishino, M.; Miyashita, S. Magnetic Properties and Metastable States in Spin-Crossover Transition of Co–Fe Prussian Blue Analogues. *J. Phys. Soc. Jpn.* **2006**, *75*, 114603. [CrossRef]
59. Gindulescu, A.; Rotaru, A.; Linares, J.; Dimian, M.; Nasser, J. Excited metastables electronic spin states in spin crossover compounds studies by atom-phonon coupling model: Gradual and two-step transition cases. *J. Appl. Phys.* **2010**, *107*, 09A959. [CrossRef]
60. Ndiaye, M.M.; Pillet, S.; Bendeif, E.; Marchivie, M.; Chastanet, G.; Boukheddaden, K.; Triki, S. Hidden Hysteretic Behavior of a Paramagnetic Iron(II) Network Revealed by Light Irradiation. *Eur. J. Inorg. Chem.* **2017**, *2018*, 305–313. [CrossRef]
61. Boonprab, T.; Lee, S.J.; Telfer, S.G.; Murray, K.S.; Phonsri, W.; Chastanet, G.; Collet, E.; Trzop, E.; Jameson, G.N.L.; Harding, P.; et al. The First Observation of Hidden Hysteresis in an Iron(III) Spin-Crossover Complex. *Angew. Chem. Int. Ed.* **2019**, *58*, 11811–11815. [CrossRef] [PubMed]
62. Fourati, H.; Bouchez, G.; Paez-Espejo, M.; Triki, S.; Boukheddaden, K. Spatio-temporal Investigations of the Incomplete Spin Transition in a Single Crystal of [Fe(2-pytrz)2{Pt(CN)$_4$}]·3H$_2$O: Experiment and Theory. *Crystals* **2019**, *9*, 46. [CrossRef]
63. Gutlich, P.; Ksenofontov, V.; Gaspar, A. Pressure effect studies on spin crossover systems. *Coord. Chem. Rev.* **2005**, *249*, 1811–1829. [CrossRef]
64. Oke, T.D.; Ndiaye, M.; Hontinfinde, F.; Boukheddaden, K. Magnetic-field induced multi-step transitions in ferromagnetic spin-crossover solids within the BEG model. *Eur. Phys. J. B* **2021**, *94*, 38. [CrossRef]
65. Ogou, S.B.; Oke, D.T.; Karimou, M.; Félix, H.; Boukheddaden, K. BEG spin-1 model with random exchange magnetic interactions for spin-crossover solids. *J. Phys. Condens. Matter* **2023**, *35*, 455704. [CrossRef] [PubMed]
66. Sotnikov, A.; Kuneš, J. Field-induced exciton condensation in $LaCoO_3$. *Sci. Rep.* **2016**, *6*, 30510. [CrossRef] [PubMed]
67. Enachescu, C.; Stoleriu, L.; Stancu, A.; Hauser, A. Competition between photoexcitation and relaxation in spin-crossover complexes in the frame of a mechanoelastic model. *Phys. Rev. B* **2010**, *82*, 104114. [CrossRef]
68. Enachescu, C.; Oetliker, U.; Hauser, A. Photoexcitation in the Spin-Crossover Compound [Fe(pic)$_3$]Cl$_2$·EtOH (pic = 2-Picolylamine). *J. Phys. Chem. B* **2002**, *106*, 9540–9545. [CrossRef]
69. Chakraborty, P.; Enachescu, C.; Hauser, A. Analysis of the Experimental Data for Pure and Diluted $[Fe_xZn_{1-x}(bbtr)_3](ClO_4)_2$ Spin-Crossover Solids in the Framework of a Mechanoelastic Model. *Eur. J. Inorg. Chem.* **2013**, *2013*, 770–780. [CrossRef]
70. Varret, F.; Boukheddaden, K.; Codjovi, E.; Enachescu, C.; Linarès, J. On the Competition Between Relaxation and Photoexcitations in Spin Crossover Solids under Continuous Irradiation. In *Spin Crossover in Transition Metal Compounds II*; Springer: Berlin/Heidelberg, Germany, 2004; Volume 234, pp. 199–229. [CrossRef]
71. Atitoaie, A.; Tanasa, R.; Enachescu, C. Size dependent thermal hysteresis in spin crossover nanoparticles reflected within a Monte Carlo based Ising-like model. *J. Magn. Magn. Mater.* **2012**, *324*, 1596–1600. [CrossRef]
72. Hauser, A.; Gütlich, P.; Hinek, R.; Spiering, H.; Schollmeyer, D. The [Fe(etz)$_6$](BF$_4$)$_2$ Spin-Crossover System—Part One: High-Spin ⇌ Low-Spin Transition in Two Lattice Sites. *Chem. A Eur. J.* **1996**, *2*, 1427–1434. [CrossRef]
73. Hauser, A.; Hinek, R.; Spiering, H.; Gütlich, P. The [Fe(etz)$_6$](BF$_4$)$_2$ Spin-Crossover System—Part Two: Hysteresis in the LIESST Regime. *Chem. Eur. J.* **1996**, *2*, 1435–1439. [CrossRef]
74. Varret, F.; Boukheddaden, K.; Chong, C.; Goujon, A.; Gillon, B.; Jeftic, J.; Hauser, A. Light-induced phase separation in the [Fe(ptz)$_6$] (BF$_4$)$_2$spin-crossover single crystal. *EPL* **2007**, *77*, 30007. [CrossRef]

75. Gudyma, I.; Maksymov, A. The cooperativity in 3D spin-crossover nanocrystals with ferromagnetic and antiferromagnetic surface. *Appl. Surf. Sci.* **2019**, *483*, 779–784. [CrossRef]
76. Erdem, R. Geometrical description of the state space in spin crossover solids with high-spin low-spin degree of freedom. *Phys. A* **2022**, *598*, 127335. [CrossRef]

Disclaimer/Publisher's Note: The statements, opinions and data contained in all publications are solely those of the individual author(s) and contributor(s) and not of MDPI and/or the editor(s). MDPI and/or the editor(s) disclaim responsibility for any injury to people or property resulting from any ideas, methods, instructions or products referred to in the content.